• U C •

FCTUC FACULDADE DE CIÊNCIAS
E TECNOLOGIA
UNIVERSIDADE DE COIMBRA

Patrícia dos Santos Oliveira

Regulation of Blood Vessel Growth

Dissertation presented to the University of Coimbra in fulfilment of the requirements necessary for obtaining a MSc degree in Biomedical Engineering

Supervisors:

Rui Travasso[1], João Carvalho[1], Orlando Oliveira[1]

[1]Centro de Física Computacional, FCTUC

Coimbra, 2014

This project was developed in collaboration with:

Centro de Física Computacional, FCTUC

Declaration of Authorship

Agradecimentos

Em primeiro lugar, quero expressar a minha gratidão para com os meus supervisores. Agradeço, em especial, ao professor Rui Travasso, por me ter guiado e encorajado ao longo deste ano. Também pela sua paciência infindável e pelo entusiasmo e dedicação cativantes que coloca nos seus projectos. Aos professores Orlando Oliveira e João Carvalho, por se terem mostrado sempre disponíveis para dar opiniões e dicas sábias.

Aos participantes das reuniões semanais do CFC, por mostrarem que da comunicação do que estamos a fazer podem surgir sinergias e novas ideias, evidenciando a importância da entreajuda.

A Coimbra e aos colegas de Engenharia Biomédica, por terem proporcionado o melhor ambiente que eu poderia imaginar para passar estes cinco anos de curso.

A todo o corpo docente do MIEB 2009-2014, pois este projecto é o culminar dos conhecimentos adquiridos ao longo do curso e por eles partilhado.

Ao Clã Luís Gomes, do Agrupamento 588-Gafanha da Nazaré, por terem sido uma fonte de força, crescimento e realização pessoal, permitindo-me ser uma pessoa mais completa. Também por terem compreendido e suportado a minha presença menos assídua ao longo deste ano.

Aos Mamutes, pelos melhores momentos de divertimento, descontração e liberdade.

Aos amigos mais próximos e ao João, por acreditarem em mim e estarem presentes em momentos únicos.

Por fim, deixo um agradecimento à família. À minha afilhada, por reclamar comigo por ainda não ter feito os trabalhos de casa. E aos meus pais, que me apoiam incondicionalmente e mais do que ninguém.

Este trabalho é financiado por Fundos FEDER através do Programa Operacional Fatores de Competitividade – COMPETE e por Fundos Nacionais através da FCT – Fundação para a Ciência e a Tecnologia no âmbito do projeto FCOMP-01-0124-FEDER-015708.

"To me programming is more than an important practical art. It is also a gigantic undertaking in the foundations of knowledge."

Grace Hopper

Abstract

Angiogenesis is a complex process where biological signals, such as the activation of signalling pathways by the binding of VEGF to its receptors at the cell membrane, are converted into mechanical forces originating cell movement. The endothelial cells then re-organize spatially into tubular structures that are able to support the flow of blood and that respond to blood pressure and shear stress by changing their number, shape and size. Therefore, a mathematical description of sprouting angiogenesis has to consider biological signals as well as relevant physical processes.

In this thesis, we model sprouting events in angiogenesis using a continuum model that takes into account the tissue elasticity and the forces exerted by the cells in the sprout. We demonstrate that the endothelial cell proliferation has to be regulated by the local mechanical stress for a well-formed vascular sprout. The force exerted at the tip cell induces an increase in the stress, which determines the locations with higher endothelial cell proliferation. The model also permits a new look into how anastomosis events are controlled by the local tissue displacements.

Our results highlight the ability of mathematical models to suggest relevant hypotheses with respect to the role of forces in sprouting, hence underlining the necessary collaboration between modelling and molecular biology techniques to improve our knowledge of the angiogenesis process.

Keywords: angiogenesis, VEGF, hybrid modelling, phase field model, elasticity, mechanical interactions, proliferation

Resumo

A angiogénese é um processo complexo capaz de originar movimento celular através da conversão de sinais biológicos em forças mecânica. Esses sinais são originados com a ligação do VEGF aos seus receptores na membrana celular. Depois disso, as células endoteliais reorganizam-se espacialmente em estruturas tubulares que são capazes de suportar o fluxo de sangue e que respondem à pressão sanguínea e *shear stress* alterando o seu número, forma e tamanho. Desta modo, uma descrição matemática da *sprouting angiogenesis* tem que ter em consideração sinais biológicos, assim como processos físicos relevantes.

Modelamos os eventos da *sprouting angiogenesis* usando um modelo contínuo que tem em conta a elasticidade do tecido e as forças exercidas pelas células no *sprout*. Para além disso, demonstramos que a proliferação das células endoteliais tem de ser regulada pelo stress mecânico local para um sprout bem formado. A força exercida na célula de ponta, chamada tip cell, induz um aumento do stress, o que determina os locais com maior proliferação endotelial. O modelo também permite um novo olhar sobre a forma como os eventos de anastomose são controlados pelos deslocamentos locais do tecido.

Os nossos resultados destacam a habilidade que os modelos matemáticos têm para sugerir hipóteses relevantes no que toca ao papel das forças no *sprouting*. É também sublinhanda a colaboração necessária entre a modelação e as técnicas de biologia molecular para melhorar o actual estado da arte.

Palavras-chave: angiogénese, VEGF, modelação híbrida, modelo de interface difusa, elasticidade, interações mecânicas, proliferação

Abbreviations

Ang-1	**A**ngiopoietin-1
Ang-2	**A**ngiopoietin-2
Dll4	**D**e**l**ta-**l**ike-4
EC	**E**ndothelial **C**ell
ECM	**E**xtra**c**ellular **M**atrix
FGF	**F**ibroblast **G**rowth **F**actor
FTCS	**F**ast-**T**ime **C**entral-**S**pace
MMPs	**M**atrix **M**etallo**P**roteinases
PDGF	**P**latelet-**D**erived **G**rowth **F**actor
VEGF	**V**ascular **E**ndothelial **G**rowth **F**actor
VEGFR2	**V**ascular **E**ndothelial **G**rowth **F**actor **R**eceptor 2

Symbols

ϕ	order parameter
F	free energy, force exerted in the tip cell
D	diffusion constant of the system
f	local free energy density
F^{el}	elastic force
ω	displacements matrix
ε	interface thickness, strain tensor
σ	stress tensor
μ	shear modulus of the system
χ	applied forces matrix
k_V	proliferation constant due to VEGF
A	applied force amplitude
r	applied force radius
V	VEGF concentration
D_g	VEGF diffusion constant
α_c	VEGF consume constant by ECs
G	shear modulus
K	bulk modulus
E	young modulus
ν	poisson's ratio
V_{max}	maximum VEFG concentration
P_{max}	maximum proliferation

List of Figures

1.1 Blood Vessels changes in response to anti-angiogenic therapy. 2
1.2 Schematic overview of vasculogenesis and angiogenesis. 4
1.3 Sprouting and intussusceptive angiogenesis: comparison between their early stages. 6
1.4 Phenotypic and molecular differences between endothelial tip and stalk cells. 7
1.5 EC's behaviour regulation through Ang1, Ang2 and VEGF. 8
1.6 Main signalling pathways that take part in angiogenesis. 9
1.7 Types of biomechanical forces on the vascular wall. 11

2.1 Free energy density curve. 19
2.2 Scheme representing the direction of forces (in black) applied to ECM (blue) and vessel (red) to create a compressive effect on the interface. 23
2.3 Topology of force field's $\mathbf{F}(x, y)$ to mimic cellular movement. 24
2.4 Topology of force field's first derivative, $\chi(x, y)$. 24

3.1 Flowchart for solving the Cahn-Hilliard equation. 30
3.2 Simulation on a 130 by 130 lattice mesh of the evolution of ϕ with $D = 1$, $\bar{\phi}_0 = -0.2$ and $dt = 0.02$, using the Cahn-Hilliard equation. . 30
3.3 Flowchart for solving the Cahn-Hilliard equation with elastic properties. 32
3.4 Simulation on a 130 by 130 lattice mesh of the evolution of ϕ with $D = 1$, $\bar{\phi}_0 = -0.2$, $\mu = 0.07$[1] and $dt = 0.02$, using the Cahn-Hilliard equation with elastic properties. 32
3.5 Flowchart for solving the Cahn-Hilliard equation with elastic properties, cell migration and chemotaxis. 35
3.6 Simulation on a 130 by 130 lattice mesh of the evolution of ϕ with $A = 5$, $r = 5$, $L_0 = 1$, $\alpha = 0.13$, $D_g = 0.9$, $\alpha_c = 0.1$ and $\mu_1 = 0.13$, using the Cahn-Hilliard equation with elastic properties, cell migration and chemotaxis. 36
3.7 Repetition of the simulation in figure (3.7) with growing of the sprout in a different direction. 36
3.8 Simulation on a 130 by 130 lattice mesh of the evolution of ϕ with proliferation coefficient $k_V = 0.05$. 37
3.9 Proliferation sites from figure 3.8. 37

4.1 Greater cell migration force, $A = 15$. 40
4.2 Smaller cell migration force, $A = 1$. 40
4.3 Greater proliferation coefficient, $k_V = 0.5$. 41
4.4 Absence of a cut-off value in $\theta(\chi)$. 41
4.5 Proliferation sites from figure 4.4. 41
4.6 Greater adhesion factor, $\alpha = 1$. 42
4.7 Regression of a sprout in favour of extension in another direction. . 43
4.8 Fusion of two tip cells. 44
4.9 ω before the fusion of two tip cells. ω functions as guidance for future work. 44
4.10 Double sprouting. Disruption of one of the sprouts. 45
4.11 Double sprouting. Disruption of the main vessel. 46

5.1 Relation of proliferation with the amount of VEGF sensed in a lattice point. 48
5.2 Results for proliferation proportional with VEGF. 51
5.3 Results for proliferation proportional with VEGF only where mechanical force exists. 51
5.4 Results for proliferation proportional with mechanical force. 52
5.5 Results for proliferation proportional with mechanical force only where VEGF exists. 52
5.6 Detailed study of each proliferation's performance. 53
5.7 New attempt to create an anastomosis with the new proliferation approach ($V_{max} = 0.1$ e $P_{max} = 0.02$). 54

List of Tables

1.1 Influence of the biomechanical forces in sprouting angiogenesis. . . . 13

2.1 Parameters used in the simulation based on biological experiments. 28

Contents

1 Introduction **1**
- 1.1 Motivation and goals . . . 1
- 1.2 Sprouting Angiogenesis . . . 4
  - 1.2.1 General aspects . . . 4
  - 1.2.2 Signalling pathways . . . 6
  - 1.2.3 Mechanical modulation . . . 11
  - 1.2.4 Overview of mathematical models . . . 14

2 Phase-field model with elasticity **17**
- 2.1 Allen-Cahn equation . . . 17
- 2.2 Conservation of the order parameter and the Cahn-Hilliard equation 18
- 2.3 Including elasticity . . . 20
- 2.4 Cell migration . . . 22
- 2.5 Chemotaxis . . . 25
- 2.6 Proliferation . . . 25
- 2.7 Parameters adjustment . . . 26

3 Computational simulation **29**
- 3.1 Cahn-Hilliard equation . . . 29
- 3.2 Elasticity . . . 31
- 3.3 Cell migration and chemotaxis . . . 31
- 3.4 Proliferation . . . 37

4 Exploring the model **39**
- 4.1 Cell migration force . . . 39
- 4.2 Proliferation . . . 40
- 4.3 Adhesion factor, α . . . 42
- 4.4 Regression . . . 42
- 4.5 Anastomosis . . . 43

5 New proliferation approach **47**

6 Conclusions and future work **55**

A Functional derivative of free energy, F (2.2) **57**

B Functional derivative of elastic force, F^{el} **59**

C Deduction of elastic energies **61**

D Functional derivative of free energy with elastic force, F (2.16) **65**

Bibliography **67**

Chapter 1

Introduction

1.1 Motivation and goals

Blood vessel growth is essential in complex animal species. Only the establishment of a vascular system guarantees the success of basic body functions. A vascular system enables the transport of oxygen and nutrients to all the body cells. Not less important is the elimination of toxic byproducts resultant from metabolic activity[2].

Not surprisingly, excessive or insufficient stimulus for vessel growth is related to the onset and progression of over 50 different diseases such as cancer, rheumatoid arthritis, diabetic retinopathy and ischemic heart disease[2,3].

Recognition that control of blood vessel growth (angiogenesis) could lead to cancer therapies stimulated intensive research in the field. While by 1970 only two manuscripts dealing with angiogenesis had been published[4], currently this number reaches more than 72 000 in total.

There are evidences that increased tumour vascularization is associated with advanced stages of various solid tumours[5]. Tumour-induced angiogenesis can persist for years, involving a disorganized, inefficient and leaky vasculature[6]. This vasculature supplies the tumour with nutrients and growth factors enabling its growth

and can be used by cancer cells that detach from the primary tumour to move and metastasize to remote organs[6,7]. Naively, one could think that starving tumours by destroying their blood supply would arrest their growth. However, after years of research, the initial work using anti-angiogenic drugs alone did not translate into long-term positive clinical results for cancer patients[8]. This is explained by the fact that a complete inhibition of angiogenesis promotes hypoxia (state of oxygen shortage) within the tumour, that can increase the occurrence of aggressive migrating tumour cell phenotypes - it is like a selection of the most aggressive types[6]. Instead, an alternative strategy has emerged: the use of anti-angiogenic drugs to normalize the tumour vasculature, thereby improving the delivery of chemotherapeutic drugs and oxygen to tumour tissues, which increases the efficiency of radiation therapy[9]. This demands treatments with specific amounts of anti-angiogenic agents (figure 1.1).

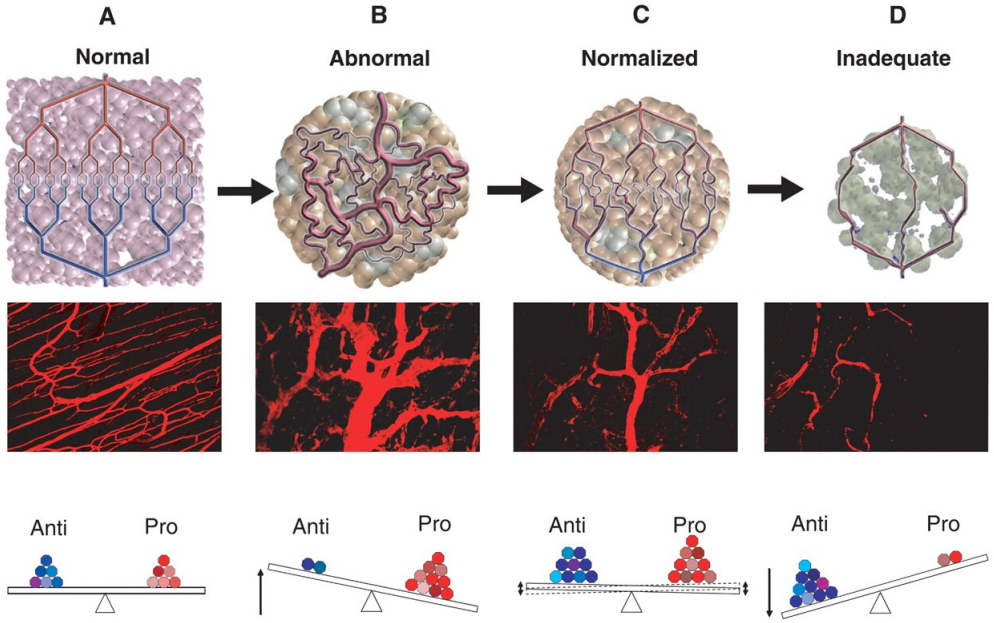

FIGURE 1.1: Blood Vessels changes in response to anti-angiogenic therapy. (a) Normal vessels. (b) Dilated, tortuous and disorganized vessels from a cancer. (c) Normalized cancer vasculature due to angiogenic inhibitors. (d) Angiogenic inhibitors can cause, eventually, the death of an increased number of vessels.[9].

Predicting the correct levels of anti-angiogenic agents that will lead to the desired results requires an in-depth understanding of both the mechanical and biological aspects of pathological angiogenesis. Our final aim is to achieve this task by

integrating the various aspects of this challenging problem through mathematical and computational modelling.

Although there was a time when computational models were developed and implemented without validation with real experiment data, nowadays this synergy between research areas is a requirement to have biological acceptance[10]. Following this, I would like to highlight the interdisciplinarity of this project. To deal with the complexity underlying the fine regulation of new blood vessel formation, we need to repeatedly traverse an iterative cycle of collaborative interaction between biology, theoretical modelling, computational simulation and experiments that directly test and parametrize the model.

We aim to understand more about the mechanical factors that mediate blood vessel formation and remodelling, because their mechanisms remain poorly understood[11]. To succeed with doing so, we use a multi-scale phase-field model that combines the benefits of continuum physics description and the capability of tracking individual cells. The first goal of this thesis is to simulate our mathematical model, which takes into account elasticity, proliferation and migration, in the C language. The next steps are to parametrize the model according to the literature, start walking towards anastomosis and include blood pressure. In order to create anastomosis, reformulations must be done in the model. For this reason, one of the first goals planned for this thesis, the inclusion of blood pressure, was substituted by improvements in the model.

Personally, I find this project a great opportunity to apply the transversal knowledge that I acquired during the Biomedical Engineering degree. Besides, numerical simulation is an important knowledge that is not confined to natural processes. In what gives respect to health, it is believed that until the end of the century computer simulation could become 'integral' in the diagnosis, treatment, or prevention of disease.

1.2 Sprouting Angiogenesis

1.2.1 General aspects

In the embryo, the primitive vasculature develops through vasculogenesis, the *de novo* blood vessel generation from vascular progenitor cells. Vasculogenesis is the earliest morphogenetic process of vascular development and occurs exclusively during the early stages of the embryonic development, allowing the organs to have the necessary oxygen to grow[12,13]. It consists of the differentiation of angioblasts (the precursors of endothelial cells) into blood islands, which then fuse to form primitive capillary plexuses[13]. These plexuses subsequently grow so as to reach another tissues (see figure 1.2). Notice that metabolically active tissues need to be closer than few hundred micrometers from a blood capillary[4]. This growth of capillaries from pre-existing microvasculature occurs through angiogenesis and is influenced by various biochemical and biomechanical factors[14].

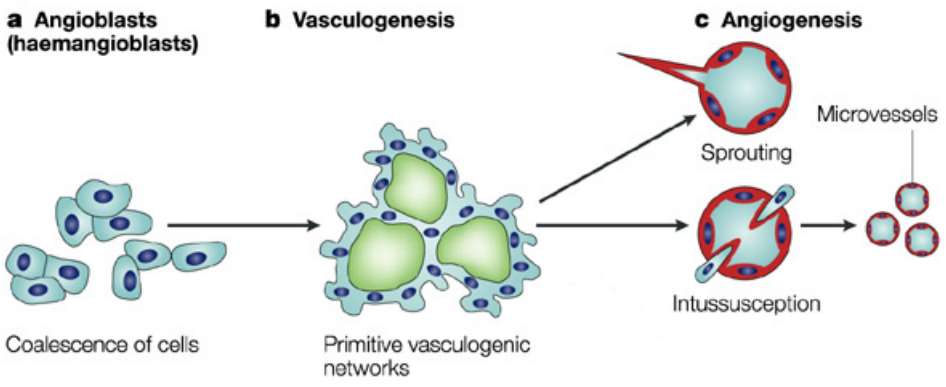

FIGURE 1.2: Schematic overview of vasculogenesis and angiogenesis. (a) Endothelial cell precursors coalesce and differentiate into endothelial cells. (b) Primitive vasculogenic networks are formed (vasculogenesis). (c) Remodelling of the networks through angiogenesis, which involves sprouting and intussusception, resulting in the formation of microvessels[15].

Angiogenesis is crucial in many physiological processes including embryonic development, wound healing, fracture repair, folliculogenesis, ovulation, pregnancy and exercise-induced vascular adaptation[13,16]. Angiogenesis is also particularly relevant in the following two important situations. First, angiogenesis occurs during tumour growth providing additional nourishment required for the tumour to

proliferate. Second, it is essential for tissue engineering purposes where is required to predict and control capillary development in scaffolds during in vitro tissue development[14,16].

Endothelial cells (ECs) constitute the inner layer of blood vessels. They have an active role in angiogenesis, being primarily responsible for capillary growth, migration, and organization of vessel lumens[6,17]. During angiogenesis, each EC residing in a vessel wall integrates local signals to determine whether it:

- remains quiescent;
- participates in vessel dilation or contraction (it may imply the EC proliferation or apoptosis, respectively);
- undergoes morphogenesis to form an angiogenic sprout or participate in intussusceptive vessel alteration[18].

The sprouting and intussusceptive ways of altering the vascular plexus are very different from each other (see figure 1.3). In sprouting angiogenesis, ECs are able to project into the extracellular matrix (ECM), disrupt the basement membrane and invade new tissues, reaching areas of tissues previously devoid of blood vessels. This is essential, for example, in wound healing. On the other hand, intussusceptive angiogenesis is much quicker. It results in the formation of two lumens from a single vessel by intravascular septation. This means there is little or no dependence on cell proliferation and migration and that is why it plays a proeminent role in vascular development in processes where growth is fast and resources are limited. Moreover, there is maintenance of organ functions because there is no need for membrane disruption[4,19].

In this work we focus on sprouting angiogenesis type. This process is better understood having been discovered nearly 200 years ago, while intussusceptive (also known as nonsprouting) angiogenesis was discovered by about two decades ago and its molecular mechanisms are not yet clearly understood[4,7]. No particular molecule has been linked to this process as opposed to, for example, VEGF for sprouting angiogenesis[7].

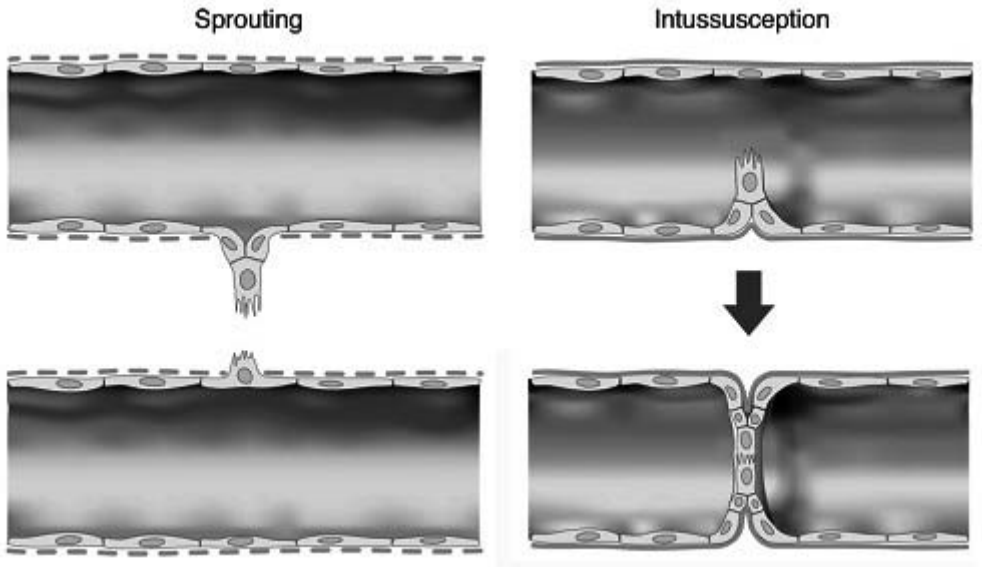

FIGURE 1.3: Sprouting and intussusceptive angiogenesis: comparison between their early stages. In sprouting angiogenesis, the disrupted membrane (dotted lines) allow ECs to migrate and proliferate to form a new vascular tube. In contrast, in intussusception the vessel wall extends into the lumen causing a single vessel to split in two, with an intact basement membrane[20].

1.2.2 Signalling pathways

Sprouting angiogenesis is initiated in poorly perfused tissues when oxygen sensing mechanisms detect a level of hypoxia that demands the formation of new blood vessels to satisfy the metabolic requirements of parenchymal cells. Most types of parenchymal cells (myocytes, hepatocytes, neurons, astrocytes, etc.) respond to a hypoxic environment by secreting a key proangiogenic growth factor called vascular endothelial growth factor (VEGF)[4]. This protein is the best studied vascular morphogen and has the ability to trigger the entire sequence of events leading to new vessel growth. It also promotes vasodilation[21]. Besides, it does not appear to exist other redundant growth factor mechanisms that are able to replace the role of VEGF in hypoxia-induced angiogenesis[4]. In the presence of VEGF, sprouting cells organize hierarchically into leading "tip" and trailing "stalk" cells. Endothelial tip cells lead sprouting vessels, extend filopodia, and migrate in response to gradients of VEGF. In contrast, adjacent stalk cells trail the tip cells, generate the trunk of new vessels, and critically maintain connectivity with parental vessels (see figure 1.4)[22].

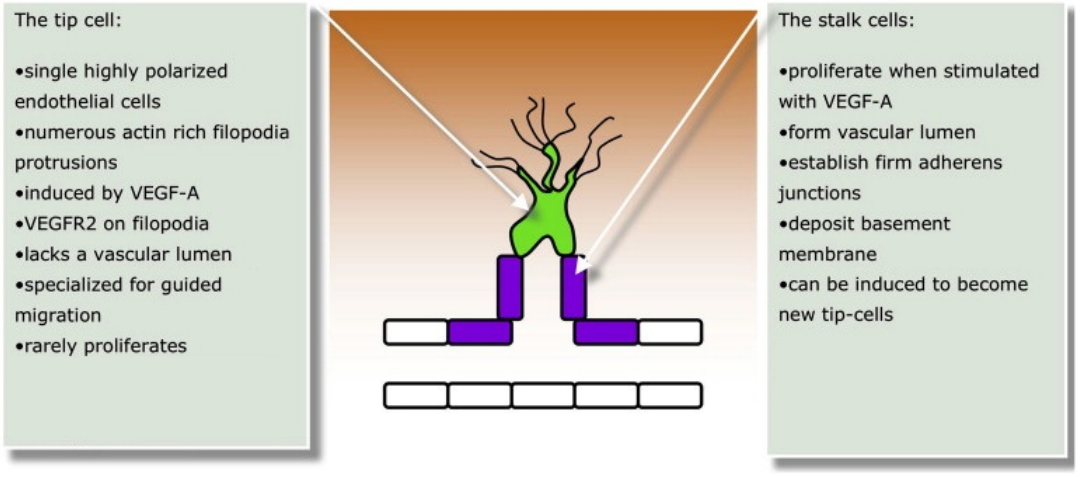

FIGURE 1.4: Phenotypic and molecular differences between endothelial tip and stalk cells. Tip cells (green) guide each vascular sprout stimulated by an extracellular VEGF gradient (orange), followed by the stalk cells (purple)[23].

Of the vast number of growth factors and signalling pathways that take part on the angiogenic cascade, angiopoietins (Ang/Tie2) and platelet-derived growth factors (PDGF-B/PGDFR-B) coordinate with VEGF to play an important regulating part in sprouting angiogenesis and maturation[24]. This can be seen either in figure 1.5 and figure 1.6.

We can divide the complex angiogenesis process in three early events before the blood flow is established: initiation, extension and maturation[24]. They are described bellow.

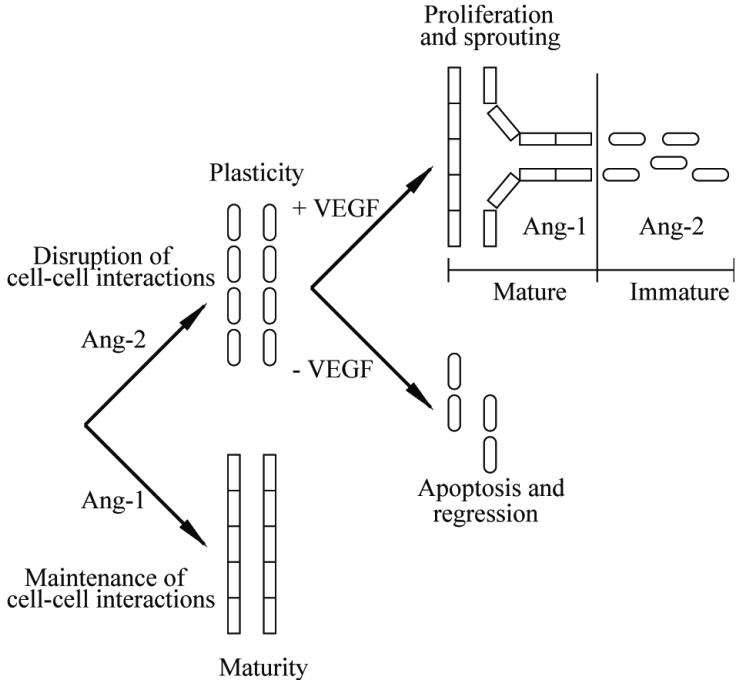

FIGURE 1.5: EC's behaviour regulation through Ang1, Ang2 and VEGF Plank et al. [25]. Overexpression of Ang1 with respect to Ang2 renders ECs quiescent and helps to maintain and stabilize mature vessels by promoting interaction between endothelial cells and supporting cells like pericytes. Conversely, the overexpression of Ang2 with respect to Ang1 blocks the stabilizing action of Ang1 by promoting the active proliferation and migration ECs in the presence of VEGF [24].

Initiation

Angiopoietins play critical roles in angiogenic outgrowth, remodelling and maturation. They are ligands for the EC-specific receptor tyrosine kinase, Tie-2 [25]. In mature vessels, ECs are covered by perycites and kept in a quiescent state by the presence of Ang1. Given a situation of hypoxia, like in some pathological cases, VEGF is produced and its binding to VEGFR2 in ECs plasma membrane triggers the production and release of Ang2 [24]. In opposition, Ang1 is expressed and produced in a constant pattern by the tissue [25]. Ang2 can have a positive or negative effect depending on the VEGF concentration in the tissue. Overexpression of Ang2 and a positive VEGF concentration lead to the detachment of pericytes, giving the necessary freedom for ECs to migrate towards the source of VEGF [24].

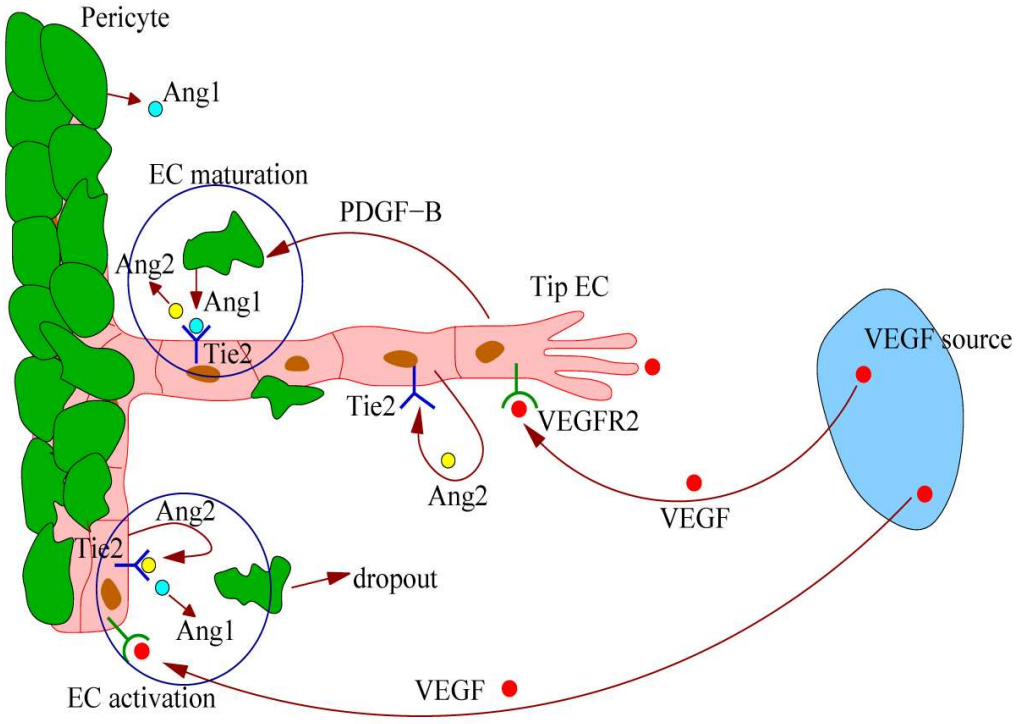

FIGURE 1.6: Main signalling pathways that take part in angiogenesis. VEGF, secreted tipically by cells in hipoxia, in particular by hipoxic tumor cells, stimulates endothelial cells to release Ang2, which dispels pericytes; it actives endothelial cells to produce PDGF-B, which induces pericyte migration towards immature vessels; pericytes generate Ang1, which mediates endothelial cell maturity.[24].

Extension

EC migration and proliferation are two of the most important activities in capillary extension. Migration is leaded by a tip cell while stalk cells follow the tip cell and proliferate, adding their daughter cells to the growing sprout[24]. Concentration of VEGF has influence on whether a cell gets the phenotype tip or stalk. Highest VEGF concentrations are associated to a tip cell phenotype[4]. The cell-cell signalling system called Delta-Notch prevents the simultaneous activation of tip cell in two neighbouring cells. In this process the Delta-Notch mechanism works as a negative feedback loop where VEGF, after binding to VEGFR2, up-regulates expression of the delta like ligand 4 (Dll4) production by tip cells. Dll4 binds to Notch receptors on neighbouring cells and results in the down-regulation of VEGFR2 receptors in the neighbour cell which dampens its migratory behaviour.[4,24,26].

Finger-like projections on tip cells called filopodia are heavily endowed with

VEGF receptors (VEGFR2), allowing them to "sense" small differences in VEGF concentrations which the ECs use to align themselves with the VEGF gradient.

ECs also secrete metalloproteinases (MMPs), which digest the ECM creating a pathway for the developing sprout. When a sufficient number of filopodia on a given tip cell have anchored to the substratum, contraction of actin filaments within the filopodia literally pull the tip cell along towards the VEGF stimulus[4,20].

Vacuoles develop and coalesce in the stalk cells forming a lumen. These stalk cells form the trunk of the newly formed capillary[4].

When the tip cells of two or more capillary sprouts converge at the source of VEGF-A secretion, the tip cells fuse together (anastomosis) to form blood-flow supporting loops[4]. Due to delta-notch mediated lateral inhibition, one of the fusing tip cells become inhibited and only one of them continues driving the vessel growth[26].

Maturation

When a local in the tissue receives adequate amounts of oxygen, VEGF-A levels return to near normal. Stabilization and maturation of vascular walls requires the recruitment of pericytes, which cover the vascular sprouts. More specifically, ECs release platelet derived growth factor-B (PDGF-B), which promotes the proliferation of pericytes and their migration towards the capillary. Pericytes produce Ang1 and its local concentration eventually balances the effect of Ang2. With Ang1 dominance and pericyte coverage, ECs begin to switch from their active phenotype back to the quiescent state, and the capillary is stabilized. Shear stress and other mechanical signals also play a role in the stabilization/maturation process[24].

1.2.3 Mechanical modulation

One should not forget that the study of mechanical forces is also crucial for understanding cell migration as is the study of the molecular players refered in 1.2.2. The movement of a cell obeys the fundamental laws of classical mechanics. As mentioned before, chemical signals can modulate cell mechanics (as is the case of the effect on the MMPs on the ECM) and, at the same time, there is plenty of evidence that mechanical forces also modulate molecular signalling through mechanochemical feedback. In addition, by having mechanical model variables, such as forces exerted by cells on their extracellular matrix, one has the ability of validating not only the biological, but also the mechanical performance of the model, in this way contributing to model fidelity[27].

Biomechanical forces imposed on the vascular wall are of three major types: tensile stress, compressive stress and shear stress (figure 1.7).

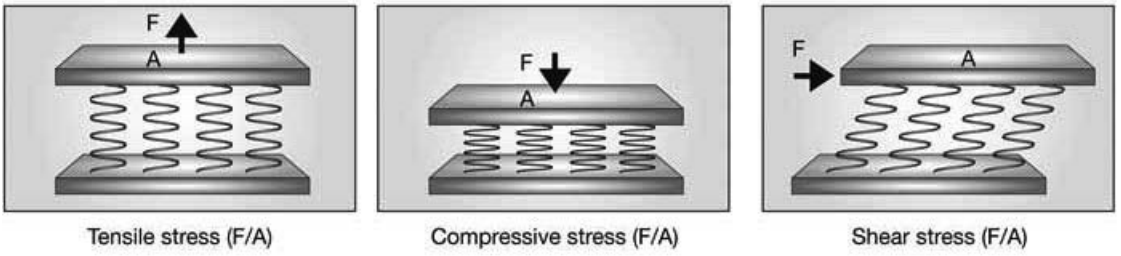

FIGURE 1.7: Types of biomechanical forces on the vascular wall. The direction of the force with respect to the surface on which it is acting determines the type of stress, which can be classified as tensile, compressive or shear stress. This stresses constantly act on the vascular wall and are due to tension along the vessel, pulsatile blood pressure and blood flow, respectively[28].

The compressive force is generated by the blood pressure and acts perpendicularly on the endothelium. The tensile force, also generated by vascular wall expansion and contraction in response to pulsatile blood pressure changes and it acts circumferential on the vessel wall to stretch the endothelial cells. Shear stress results from blood flow and is a product of fluid viscosity and the velocity gradient between adjacent layers of the blood flow[29]. It also induces EC shape change such that the long axis of the cell body aligns with the direction of flow[30].

Factors like blood flow, stretch of capillaries (as a result of muscle activity[30]), ECM stiffness and fluid forces have influence in the intensity of this biomechanical forces. The explanation of their positive/negative influence in angiogenesis can be seen on table 1.1.

Factor	Greater	Smaller
Blood flow	The greater the blood flow (consequently, a greater shear stress) the greater is the proliferation of endothelial cells, thus creating more sprouts[30].	Capillaries with slow flow gradually narrow and disappear[30].
Stretch	Stretching of endothelial cells induces cell division and proliferation in the presence of soluble growth factor[29].	Non-stretched cells remain spherical in shape, exhibit cell-cycle arrest or even undergo apoptosis[29].
ECM stiffness	The greater the substrate stiffness is, the greater is the projected area of ECs. It promotes the generation of traction force. The ECs prefer cell-substrate connections than cell-cell connections, migrating away from each other[31].	In extremely soft ECM gels, cells may undergo apoptosis if they cannot develop a sufficient amount of tension that is necessary for shape stability and survival.[30].
Fluid forces	Interstitial flow directs sprouts to other vessels, against the direction of interstitial flow, and consequently, toward vessels that have higher microvascular pressure than their own[18].	Sprouts are not redirected to other vessels.

TABLE 1.1: Influence of the biomechanical forces in sprouting angiogenesis.Blood flow and stretch due to exercise influence proliferation of ECs positively and ECM stiffness promotes migration. On the other hand, the smaller they are the larger is the possibility for ECs to undergo apoptosis. Interstitial fluid pressure, a solution that bathes and surrounds the cells, directs sprouts to other vessels.

1.2.4 Overview of mathematical models

Mathematical modelling of angiogenesis has been gaining importance as a means of predicting sprout and growth of new vessels and/or branching/anastomosis, in response to one or more stimulatory or inhibitory factors. Therefore, a variety of models has been developed for the last 20 years, each focusing on different aspects of the angiogenesis process and occurring at different biological scales - ranging from the molecular to the tissue levels. Those models can be divided into three categories: continuum, discrete and hybrid[16,26,30].

Continuum models aim to describe the large-scale, average behaviour of cell populations. They use partial and ordinary differential equations (PDEs/ODEs) to describe the variation of dependent variables in space and time. One of their advantages is that they can be discretized with standard finite difference or finite element methods. The continuous approach provides valuable insight into the processes of angiogenesis but they are limited in their prediction of the structure of vascular networks[6,16,30].

With discrete methods, the motion of individual ECs can be tracked over time, and the movement is generally based on a set of rules. They use a discrete approximation in terms of the state of cells, time evolution, and/or space[30]. These models offer unique capability of representing and interpreting blood vessel growth pattern and, compared to models based on continuous PDEs, discrete models are computationally more efficient[16,30]. Although, with the number of rules and interactions that need to be expressed for every cell, the model can get very complex and difficult to control. Another difficulty remains with the fact that most of the parameters must be linked to experimental observables, a process not so simple.

Often, discrete modelling of individual cells is combined with continuous modelling of the ECM and diffusing solutes (like VEGF, MMPs and fibronectin), resulting in a hybrid model and providing appropriate computational resolution across various scales[16]. Das et al. (2010) developed a three-dimensional model for angiogenesis, where each EC is modelled as an individual decision-making entity that

can follow one of several state trajectories: quiescence, proliferation, migration or apoptosis. The decision is stochastic (probability based) and is a function of its current state, the condition of the surrounding matrix and external governing factors, e.g., the growth factors present in neighbouring matrix. It takes into account mechanical factors such as the presence or absence of flow and initial matrix stiffness. The mechanical factors have a global effect, in opposition with variables like growth factor concentrations that only affect the local environment, making this an example of an hybrid approach[14].

Another hybrid approach, more similar to our model, is the one recently proposed by van Oers et al.[32]. It is capable of describing the contractile forces that endothelial cells exert on the ECM, the resulting strains in the ECM and the cellular response to the strains, suffices for reproducing the behaviour of individual endothelial cells and the interactions of endothelial cell pairs in compliant matrices.

Despite the variety of approaches that can be done, I consider that one must not forget two important things while developing a model for angiogenesis: to make it easy to include more angiogenic factors and also to keep the ability to cross-talk with experimental results.

For an in-depth report on recent work in the modelling and simulation of sprouting angiogenesis I refer to the recent article of review done by Heck et al. (2014)[27] and references within. In the end, they conclude that there is space to improve the actual models by extending them with a proper description of cell and matrix mechanics, because this aspect has received, so far, little attention.

The present work of perfecting a model of angiogenesis is a step forward to the aim of using computer simulation in the diagnosis, treatment and prevention of disease. It is predicted that this technology will be integral to the way clinical decisions are made in operating theaters by the end of the century[33]. We are still many years away from this, but each increment we make in models for physiological processes such as angiogenesis, relevant in disease, is a step closer.

Chapter 2

Phase-field model with elasticity

2.1 Allen-Cahn equation

We will model angiogenesis as a system with two phases (endothelial tissue and extracellular matrix) studying their shape as a whole but not discarding the possibility to track individual cells. As said in section (1.2.4), having a hybrid approach requires less computational effort than dealing with every cell individually. Following a phase-field model, we can modify the governing equations to incorporate some of the physical effects that are believed to govern the structure of a thin interface[34].

Our starting point for a theory of phase ordering (and separation) kinetics is Allen-Cahn partial differential equation:

$$\frac{\partial \phi(\mathbf{r},t)}{\partial t} = -D\frac{\delta F[(\phi(\mathbf{r},t))]}{\delta \phi(\mathbf{r},t)} \tag{2.1}$$

We have $\phi(\mathbf{r},t)$ as the system's order parameter in point r, time t, which distinguish the two phases. The evolution of this order parameter depends on the system's free energy $F[\phi(\mathbf{r},t)]$. The constant D refers to the diffusion of our system and the minus signal it's due to the fact that we want to minimize the

system's energy. This is the deterministic version of the stochastic Ginzburg-Landau equation. By having a deterministic equation as the basis of our model, we know that in the same conditions we must always get the same solution, which is useful to study the effect of any change we make in our system.

The local dynamics of the system (the dynamics of an isolated cell) is governed by the relaxational mechanism driven by the free-energy functional

$$F[\phi(\mathbf{r},t)] = \int \left[f(\phi(\mathbf{r},t)) + \frac{\varepsilon^2}{2}(\bigtriangledown\phi(\mathbf{r},t))^2 \right] d\mathbf{r}, \tag{2.2}$$

where $f(\phi(r,t))$ is the local free energy density that can be manipulated to give us different values for the phases' domains. Here, the second term of the integral is an energetic penalty for the variation of ϕ and forces the interface's perimeter to minimize. ε is the weight of this penalty.

The local free energy density used is:

$$f(\phi) = \frac{\phi^4}{4} - \frac{\phi^2}{2} \tag{2.3}$$

As we want to minimize the free energy functional, we observe that this happens when the system has two homogeneous phases at $\phi = \pm 1$ (2.1).

After calculating the derivative of the functional F (see the steps in A), we can make the substitution in (2.1), obtaining the Allen-Cahn equation:

$$\frac{\delta\phi}{\delta t} = D\left[\phi - \phi^3 + \varepsilon^2\nabla^2\phi\right]. \tag{2.4}$$

2.2 Conservation of the order parameter and the Cahn-Hilliard equation

The quantity of ϕ can flow or move but we do not want it to disappear, i.e. we want to conserve the integral $\int \phi(\mathbf{r},t)\, d\mathbf{r}$. Therefore, we need to have a continuity

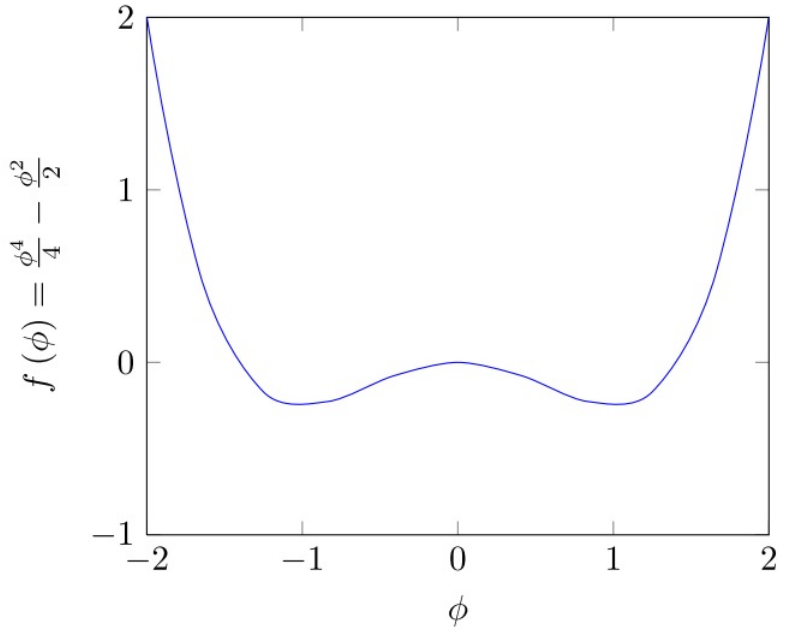

FIGURE 2.1: Free energy density curve. We can observe the double well shape of $f(\phi)$ where the minima corresponds to the two pure phases.

equation in the basis of our diffusion equation. Continuity equations have the following form:

$$\frac{\delta\phi}{\delta t} + \nabla \cdot \mathbf{j} = 0 \tag{2.5}$$

where $\mathbf{j}$ is the flux. In other words, $\mathbf{j}$ is the amount of ϕ per unit time, that crosses a unit area, and it's given by:

$$\mathbf{j} = -D\ \nabla \frac{\delta F}{\delta \phi} \tag{2.6}$$

Replacing (2.6) in (2.5):

$$\frac{\delta\phi}{\delta t} = D\ \nabla^2 \left[\phi - \phi^3 + \varepsilon^2 \nabla^2 \phi\right] \tag{2.7}$$

enables the mean value of the order parameter to remain constant throughout the simulation, as we wanted. This is the Cahn-Hilliard equation.

2.3 Including elasticity

We consider the following strain (2.8) and stress (2.9) tensors, for isotropic and homogeneous materials:

$$\varepsilon_{ij} = \frac{1}{2}\left(-\partial_j u_j + \partial_j u_j\right) \tag{2.8}$$

$$\sigma_{ij} = K\varepsilon_{kk}\delta_{ij} + 2\mu\left(\varepsilon_{ij} - \frac{1}{d}\varepsilon_{kk}\delta_{ij}\right) \tag{2.9}$$

The elastic field $\mathbf{u}(\mathbf{r}, t)$ is the displacement vector measured at a certain position $\mathbf{r}$ and time t. We also have ε_{kk} as the trace of the strain tensor, associated to the volume variation, and δ_{ij} as the Kronecker symbol. The bulk modulus is represented by K, the dimensionality of the system by d, and the shear modulus by μ. We consider that K and d are constants of the system (d is two as we are working in 2D), and that the shear modulus is dependent on ϕ, having the following relation:

$$\mu = \mu_0 - \mu_1\phi,$$

where $\mu_1 << \mu_0$, i.e. the capillary phase, with $\phi = 1$, has a lower shear modulus than the ECM.

The first step is to include the elastic force F^{el} in the free energy expression.

$$F^{el} = \int \frac{1}{2}\sigma_{ij}\varepsilon_{ij}\ d\mathbf{r} \tag{2.10}$$

$$F[\phi] = \int \left[f(\phi) + \frac{\varepsilon^2}{2}(\bigtriangledown\phi)^2 + F^{el}\right]\ d\mathbf{r} \tag{2.11}$$

The elastic force can be written in order to $\mathbf{u}(\mathbf{r}, t)$ as:

$$\begin{aligned}
F^{el} &= \int \frac{1}{2}\left(K\varepsilon_{kk}\delta_{ij} + 2\mu\left(\varepsilon_{ij} - \frac{1}{d}\varepsilon_{kk}\delta_{ij}\right)\right)\varepsilon_{ij}\ d\mathbf{r} \\
&= \int \frac{1}{2}\left(K\varepsilon_{kk}^2 + 2\mu\varepsilon_{ij}\varepsilon_{ij} - \frac{2\mu}{d}\varepsilon_{kk}^2\right)\ d\mathbf{r} \\
&= \int \frac{1}{2}\left[\left(K - \frac{2\mu}{d}\right)(\partial_i u_i)^2 + \frac{2\mu}{4}(\partial_i u_j + \partial_j u_i)(\partial_i u_j + \partial_j u_i)\right]\ d\mathbf{r} \\
&= \int \frac{1}{2}\left[\left(K - \frac{2\mu}{d}\right)(\partial_i u_i)^2 + \mu(\partial_i u_j \cdot \partial_i u_j + \partial_i u_j \cdot \partial_j u_i)\right]\ d\mathbf{r}.
\end{aligned}$$

After calculating our functional derivative (the steps are described in Appendix B) we conclude that:

$$\frac{\delta F^{el}}{\delta u_i} = -\partial_j \sigma_{ij} = -\nabla\sigma \tag{2.12}$$

The mechanical equilibrium of the system is given by $\nabla\sigma + \mathbf{f}_{ext} = 0$, where $\mathbf{f}_{ext}$ is the density of applied body forces in the system. Therefore, in our system,

$$\frac{\delta F^{el}}{\delta \mathbf{u}_i} - \mathbf{f}_{ext} = 0. \tag{2.13}$$

From this equation we extend the free energy to include the body forces. These body forces correspond to the sum of the adhesion forces (proportional to $\bigtriangledown\phi$), and the force exerted by the tip cell. Thus, the last force is supposed to vary much faster than ϕ and is considered as a constant field:

$$F[\phi, \mathbf{r}] = \int \left[f(\phi, \mathbf{r}) + \frac{\varepsilon^2}{2}(\bigtriangledown\phi(\mathbf{r}, t))^2 + F^{el} - \chi \bigtriangledown \mathbf{u}(\mathbf{r}, t) \right] d\mathbf{r} \tag{2.14}$$

where $\bigtriangledown\chi = -\mathbf{f}_{ext}$.

Here χ is given by the sum of the tip and adhesion contributions;

$$\bigtriangledown \chi = \bigtriangledown(\chi^{adh} + \chi^t) = -\alpha \bigtriangledown \phi - f^t_{ext}, \tag{2.15}$$

where α is a constant that characterizes adhesion and f^t_{ext} is the force density exerted by the tip cell. Hence we have that $\chi^{adh} = -\alpha\phi$ and we obtain χ^t in practice by solving $\bigtriangledown\chi^t = -f^t_{ext}$.

After solving the zeroth and first order elastic energies (see Appendix C), we can substitute them in 2.11:

$$F_{el}{}^0 = \int \frac{-\chi^2}{2\left(K - \frac{2\mu_0}{d} + 2\mu_0\right)}\, d\mathbf{r}$$

$$F_{el}{}^1 = \int \left[\frac{\mu_1\phi}{d}\partial_{ii}\omega\partial_{jj}\omega - \mu_1\phi\partial_{ij}\omega\partial_{ij}\omega \right] d\mathbf{r}$$

$$F[\phi] = \int \left[f(\phi) + \frac{\varepsilon^2}{2}(\bigtriangledown\phi)^2 + \frac{-\chi^2}{2\left(K - \frac{2\mu_0}{d} + 2\mu_0\right)} + \frac{\mu_1\phi}{d}\partial_{ii}\omega\partial_{jj}\omega - \mu_1\phi\partial_{ij}\omega\partial_{ij}\omega \right] d\mathbf{r} \tag{2.16}$$

In Appendix D we reach the expression for the functional derivative of F. Therefore, the Cahn-Hilliard equation can finally be modified in order to consider the elastic properties of the system:

$$\begin{aligned} \frac{\partial\phi}{\partial t} = \bigtriangledown^2 \left[-\phi + \phi^3 - \varepsilon^2 \bigtriangledown^2 \phi + \frac{\alpha\chi}{L_0} - \mu_1 \left(\partial_{ij}\omega\partial_{ij}\omega - \frac{1}{d}(\bigtriangledown^2\omega^2) \right) \right] + \\ + 2\frac{\mu_1\alpha}{L_0} \left[\frac{\phi}{d} \bigtriangledown^2 (\phi \bigtriangledown^2 \omega) + \partial_{ij} (\phi\partial_{ij}\omega) \right] \end{aligned} \tag{2.17}$$

where $\bigtriangledown^2\omega = \frac{-\alpha\phi+\chi^t}{L_0}$.

We can easily see that if the elastic constant μ_1 is zero we nullify the elastic terms and go back to Cahn-Hilliard equation.

2.4 Cell migration

In a physical perspective, the movement of the tip cell can be understood as a force centred on the interface between cell membrane and ECM (see figure 2.2). In fact, there's no difference on whether the force is compressive or distensive. As our domains have different rigidity, the softer domain will always be the one to move to compensate the perturbation, regardless of its compressive or distensive nature. Alterations in the rigid domain are more expensive in terms of energy.

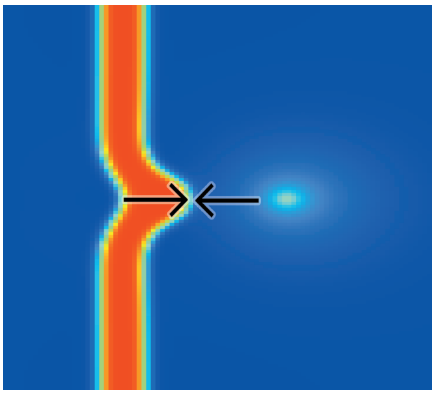

FIGURE 2.2: Scheme representing the direction of forces (black arrows) applied to ECM (blue) and vessel (red) to create a compressive effect on the interface. Net movement is made in the direction of the source of VEGF (light blue). The softer phase occupies the deformed region in order to compensate the perturbation.

We model the force that pulls the tip cell $\mathbf{F}(x, y)$, centred in the coordinates x_0 and y_0, as the first derivative of a 2D gaussian with an amplitude A and radius r,

$$\mathbf{F}(x,y) = A\frac{d}{dx}\left(e^{\frac{-(x-x_0)^2+(y-y_0)^2}{r^2}}\right)\hat{\imath},$$

and χ comes from the relation:

$$\bigtriangledown^2\chi^t = -\bigtriangledown\cdot\mathbf{F} = -(\partial_x F_x + \partial_y F_y),$$

where $\partial_y F_y = 0$ because the force is being applied in the horizontal direction. $\mathbf{F}$ mimics the unbalanced and polar distribution of forces across the cell-surface contact area during cell migration (see figure 2.3)[35].

In order to obtain the force field's gradient the following second derivative is calculated:

$$\left(e^{-\frac{(x-x_0)^2}{r^2}}\right)'' = -\left[\frac{4(x-x_0)^2}{r^4} - \frac{2}{r^2}\right]e^{-\frac{(x-x_0)^2}{r^2}}$$

which gives

$$\bigtriangledown\cdot\mathbf{F} = -A\left[\frac{4(x-x_0)^2}{r^4} - \frac{2}{r^2}\right]e^{-\frac{(x-x_0)^2+(y-y_0)^2}{r^2}}. \tag{2.18}$$

We may want to apply the force in another direction, other than the horizontal one. In order to do so, we multiply the coordinates for the rotational matrix. New

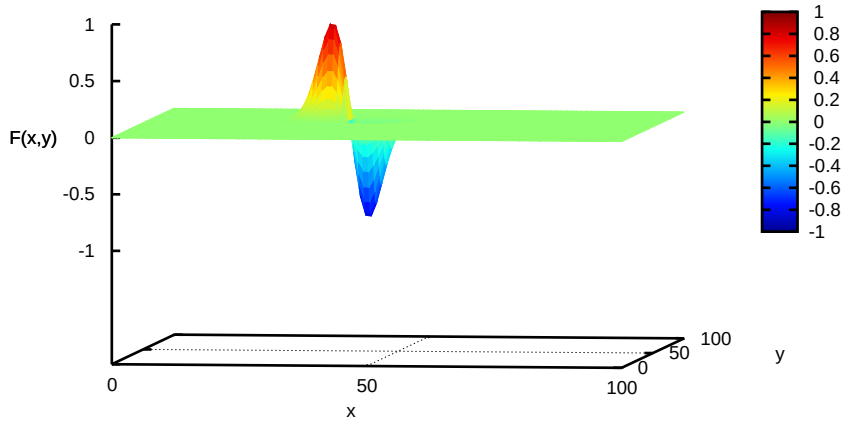

FIGURE 2.3: Topology of force field's $\mathbf{F}(x, y)$ with $r = 5$ and $A = 1$ to mimic cellular movement; in this case the cell is moving in the x direction.

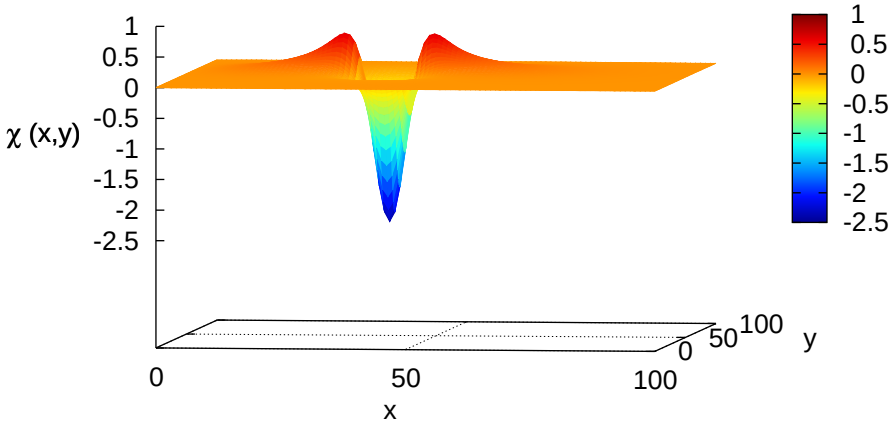

FIGURE 2.4: Topology of force field's first derivative, $\chi(x, y)$, with an amplitude $A = 5$. The negative values of χ represent a compression zone while the positive values represent distension zones. Distension zones occur in the capillary just before the tip cell and in the ECM just after the tip cell.

coordinates are substituted in (2.18).

$$\begin{bmatrix} (x-x_0)' \\ (y-y_0)' \end{bmatrix} = \begin{bmatrix} cos(\theta) & -sin(\theta) \\ sin(\theta) & cos(\theta) \end{bmatrix} \begin{bmatrix} x-x_0 \\ y-y_0 \end{bmatrix} = \begin{bmatrix} (x-x_0)cos(\theta) - (y-y_0)sin(\theta) \\ (x-x_0)sin(\theta) + (y-y_0)cos(\theta) \end{bmatrix}$$

2.5 Chemotaxis

To provide the cues for the migration direction we must take into account chemotaxis. We consider the presence of the most common growth factor VEGF, in the soluble state, and term it V. We model its concentration through the ECM with the following equation:

$$\frac{\partial V}{\partial t} = D_g \bigtriangledown^2 V - \alpha_c \theta(\phi) V, \tag{2.19}$$

which basically is the difference between the migration by diffusion and the consumption by the endothelial cells. We have D_g as the diffusion constant of VEGF, which is consumed by the EC's at a rate α_c. The Heaviside step function allows us to say if there is consumption of VEGF or not (it only happens inside the capillary).

$$\theta(\phi) = \begin{cases} 0 \text{ if } \phi < 0 \text{ (outside the capillary)} \\ 1 \text{ if } \phi > 0 \text{ (inside the capillary)} \end{cases}$$

2.6 Proliferation

Angiogenesis also has a proliferative portion which is influenced by both the mechanical stimulus and the growth factor concentration[36]. Thus, any new material added to the system would have to be dependent on these factors. Therefore, the proliferation term is given by:

$$(1-\phi)\theta(1-\phi)(\theta(\phi)\theta(\chi)k_V V), \tag{2.20}$$

where k_V is the proliferation constant due to the concentration of V.

In order to mimic cell division, we want to add new matter to areas adjacent to where vessel matter already exists. As we do not want to have new material being added inside the vessel, where $\phi = 1$, we use $(1 - \phi)$. It dampens the proliferative effect for increasing ϕ, preventing fluctuations inside the pure domain (i.e. $\phi > 1$ instead of $\phi = 1$)). With $\theta(1 - \phi)$ we totally eliminate the division effect for local values of $\phi > 1$[36].

In $\theta(\phi)\theta(\chi)k_V V$, we use the Heaviside step function to nullify the proliferation terms for negative values of ϕ and negative values of χ (corresponding to compression sites). This means we will have proliferation when V is positive, χ is positive, and both happen inside the vessel.

Finally, our state equation is:

$$\begin{aligned}\frac{\partial \phi}{\partial t} = \bigtriangledown^2 \left[-\phi + \phi^3 - \varepsilon^2 \bigtriangledown \phi - \frac{\alpha \chi}{L_0} - \mu_1 \left(\partial_{ij}\omega \partial_{ij}\omega - \frac{1}{d}(\bigtriangledown^2 \omega^2) \right) \right] + \\ + 2\frac{\mu_1 \alpha}{L_0} \left[\frac{\phi}{d} \bigtriangledown^2 (\phi \bigtriangledown^2 \omega) + \partial_{ij} (\phi \partial_{ij}\omega) \right] + \\ + (1 - \phi)\theta(1 - \phi)(\theta(\phi)\theta(\chi)k_V V) \end{aligned} \tag{2.21}$$

2.7 Parameters adjustment

Having talked about the importance of basing the model on biological experiments, before adding any improvement we cannot forget this point. Hence, urges the necessity of making a thorough research for all the parameters we have in the simulation.

In what gives respect to elasticity, μ_1 and μ_0 are constants relatively easy to calculate based on literature values. It depends on shear modulus, G, of ECM and ECs:

$$\mu_0 = \frac{G_{EC} + G_{ECM}}{2} \tag{2.22}$$

and

$$\mu_1 = \frac{G_{EC} - G_{ECM}}{2}. \tag{2.23}$$

Although it may be hard to find values for G, we are dealing with two homogeneous isotropic linear elastic materials. This means that given two elastic moduli for each one, the others can be calculated. After knowing μ_0 we can get the value of L_0:

$$L_0 = \bar{K} + \mu_0, \tag{2.24}$$

where $\bar{K}$ is the average bulk modulus between ECM and ECs.

The search on elastic moduli was made having in mind that, preferably, both should be found in the same reference. In this way, we assure that they were obtained in the same conditions. Young modulus, E and Poisson's ratio, ν were found for both ECM and ECs. Therefore, G and K can be calculated according to

$$G = \frac{E}{2(1+\nu)} \tag{2.25}$$

and

$$K = \frac{E}{3(1-2\nu)}. \tag{2.26}$$

The value found for the protrusion force per area, F, was recently used in a continuous model for angiogenesis, developed by Zheng et al.[24]. The amplitude of χ, can then be obtained with

$$A = \frac{F}{L_0}. \tag{2.27}$$

Despite the fact that there is no information on literature about proliferation rates, we collected from IBILI[1]'s experiments a value for k_V.

We also searched for the average length of an EC, d_{EC}. We consider that we are working with monolayer capillaries, which means that the diameter of the initial capillary is equal to the EC diameter.

Values found and calculated are presented in the next page's table.

[1]IBILI is the Institute for Biomedical Imaging and Life Sciences, a research Institution of the Faculty of Medicine – University of Coimbra

Variable	Value	Source
E_{EC}	$4 \times 10^{-10} \frac{N}{\mu m^2}$	Feneberg et al.[37]
ν_{EC}	0.49	Califano and Reinhart-King[38]
G_{EC}	$1.34 \times 10^{-10} \frac{N}{\mu m^2}$	equation 2.25
K_{EC}	$6.67 \times 10^{-9} \frac{N}{\mu m^2}$	equation 2.26
E_{ECM}	$3 \times 10^{-9} \frac{N}{\mu m^2}$	Raub et al.[39]
ν_{ECM}	0.13	Raub et al.[39]
G_{ECM}	$1.33 \times 10^{-9} \frac{N}{\mu m^2}$	equation 2.25
K_{ECM}	$1.35 \times 10^{-9} \frac{N}{\mu m^2}$	equation 2.26
μ_0	$7.30 \times 10^{-10} \frac{N}{\mu m^2}$	equation 2.22
μ_1	$5.97 \times 10^{-10} \frac{N}{\mu m^2}$	equation 2.23
L_0	$4.74 \times 10^{-9} \frac{N}{\mu m^2}$	equation 2.24
$\frac{\mu_1}{L_0}$	0.13	-
F	$1 \times 10^{-8} \frac{N}{\mu m^2}$	Zheng et al.[24]
A	2.1	equation 2.27
d_{EC}	10 μm	Plank et al.[25]
k_V	0.05	IBILI

TABLE 2.1: Parameters used in the simulation based on biological experiments.

The value for E_{ECM} was chosen from an interval of values that went from 500 PA to 12 000 PA.

The values proposed are reference parameters. In the simulations we may use slightly different values.

Chapter 3

Computational simulation

For a better understanding of the model, the computational simulation is explained in this chapter step-by-step, along with flowcharts and graphical results.

3.1 Cahn-Hilliard equation

We simulate the Cahn-Hilliard equation with FTCS (Forward-Time Centred-Space (2.4)).

In order to do that, we first discretize the laplacian operator with a finite difference scheme:

$$\bigtriangledown^2 \phi(i,j) = \phi(i+1,j) + \phi(i-1,j) + \phi(i,j+1) + \phi(i,j-1) - 4\phi(i,j). \quad (3.1)$$

The laplacian operator is then applied to the term between square brackets in equation 2.4. Finally, the solution of ϕ^{t+dt} can be obtained:

$$\phi^{t+dt} = \phi^t + dtD\nabla^2 \left[\phi - \phi^3 + \varepsilon^2\nabla^2\phi\right]. \quad (3.2)$$

Periodic boundaries are always considered. This means the neighbour of a point at the boundary is at the opposite boundary.

The algorithm's structure is expressed in the flow diagram below.

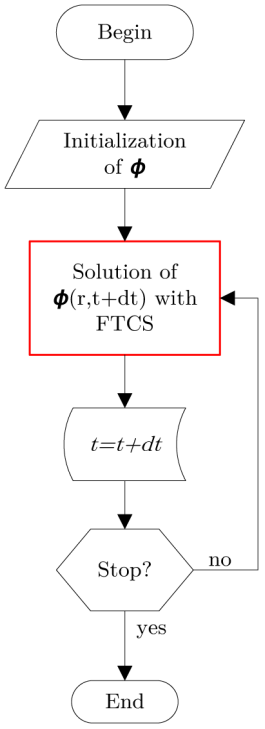

FIGURE 3.1: Flowchart for solving the Cahn-Hilliard equation. After initializing ϕ with random values near -0.2[1], the solution of ϕ in the present instant, t, is calculated with FTCS, as explained above. After updating time, $t + dt$, the same steps are repeated until we reach the stop condition (when $t = t_{max}$).

In the simulation we see the evolution from a disordered state to the formation of ordered domains well separated (see figure (3.2)). This arises directly from particles of the same type reorganizing themselves spatially to minimise the systems free energy[36].

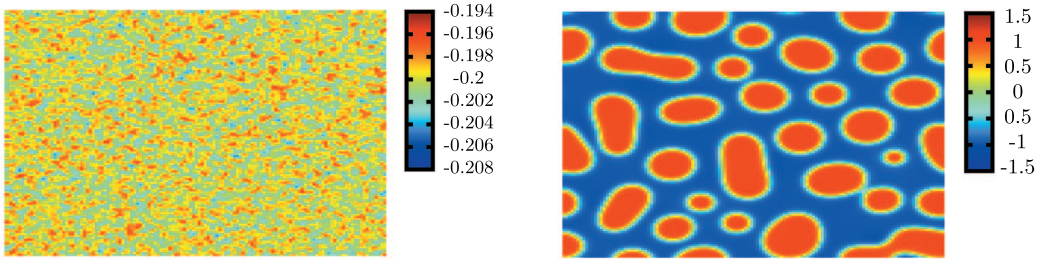

(a) (b)

FIGURE 3.2: Simulation on a 130 by 130 lattice mesh of the evolution of ϕ with $D = 1$, $\bar{\phi}_0 = -0.2$ and $dt = 0.02$, using the Cahn-Hilliard equation, for (a) 0; (b) 33000 iterations. In (a) we can observe the initial ϕ, with random values near -0.2. In (b), the interface is visible (yellow/green). Notice the formation of droplets of soft-phase (red) over a hard domain (blue).

3.2 Elasticity

To model our system with elasticity (2.17), we first need to calculate the displacements matrix, ω. With the Jacobian relaxation method:

$$\omega(i,j)^{(n+1)} = \omega(i,j)^{(n)} + \frac{1}{4}\left[\omega(i+1,j)^{(n)} + \omega(i-1,j)^{(n)} + \omega(i,j+1)^{(n)} + \omega(i,j-1)^{(n)} - \right.$$
$$\left. -4\omega(i,j)^{(n)} + \frac{\alpha\phi(i,j)}{L_0}\right],$$

considering that our lattice distance is one, either in the horizontal and vertical direction. We iterate until we converge into the solution. This means, until the difference between two successive iterations is insignificant. This equation is solved under the boundary condition that the spatial average volume of ω is zero.

After calculating ω we do its derivatives:

$$\partial_{ij}\omega\partial_{ij}\omega = \partial_{xx}\omega\partial_{xx}\omega + \partial_{xy}\omega\partial_{xy}\omega + \partial_{yx}\omega\partial_{yx}\omega + \partial_{yy}\omega\partial_{yy}\omega \quad \text{and}$$
$$\partial_{ij}(\phi\partial_{ij}\omega) = \partial_{xx}(\phi\partial_{xx}\omega) + \partial_{xy}(\phi\partial_{xy}\omega) + \partial_{yx}(\phi\partial_{yx}\omega) + \partial_{yy}(\phi\partial_{yy}\omega).$$

The greater is the elasticity constant (μ_1), the greater is the capability of the soft material to deform itself and bridge close phases of the same value (see figure 3.4). This way, we prevent the system to form round domains as before.

3.3 Cell migration and chemotaxis

As the direction of migration is determined by the presence of growth factors, it makes sense to include chemotaxis together with cell migration.

In practice, our growth factors are 2D gaussians with value 1 in the center. We initialize a matrix, V, with the location and number of fonts we find appropriate. In each iteration, we calculate its diffusion (2.19). The value in the center is maintained.

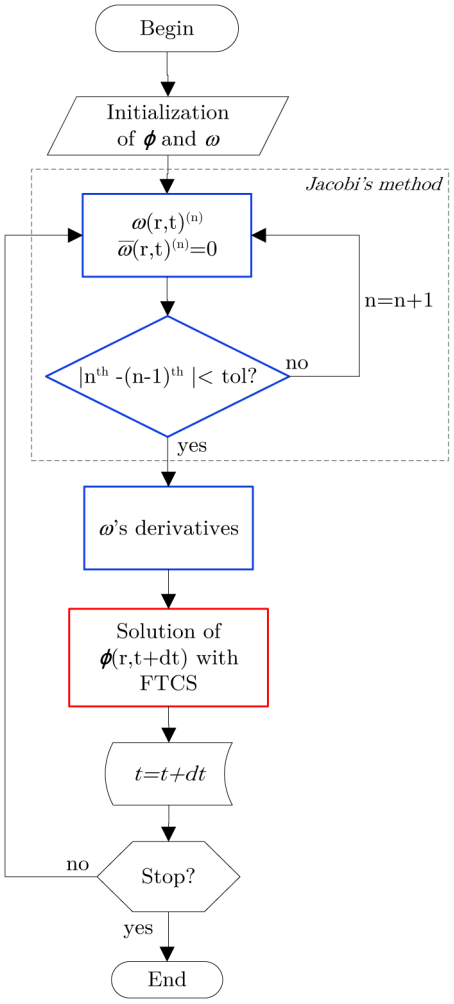

FIGURE 3.3: Flowchart for solving the Cahn-Hilliard equation with elastic properties. Like ϕ, ω is initialized with random values near zero. The new value of ω is obtained with successive iterations of the Jacobi's method, until the error between the iteration n^{th} and $(n+1)^{th}$ is smaller than the tolerance. W's derivatives are used to calculate the solution of ϕ in the instant t.

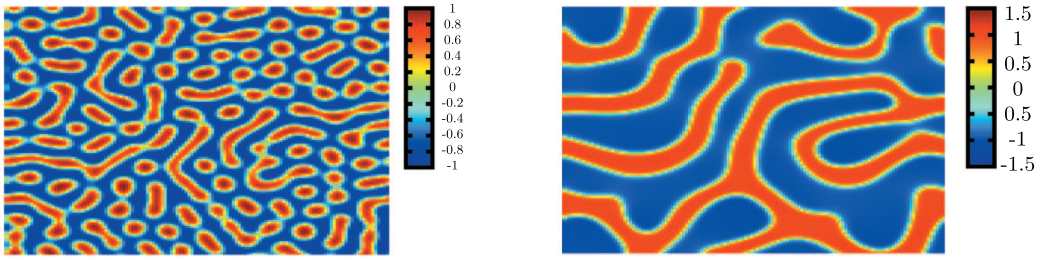

(a) (b)

FIGURE 3.4: Simulation on a 130 by 130 lattice mesh of the evolution of ϕ with $D = 1$, $\bar{\phi}_0 = -0.2$, $\mu = 0.07$[1] and $dt = 0.02$, using the Cahn-Hilliard equation with elastic properties, for (a) 3000; (b) 33000 iterations. The network of interconnected soft-phase (red) formed over the hard-phase (blue) is observable.

In angiogenesis, an EC gets the tip phenotype when VEGF binds to VEGFR2. In our case, the "tip cell" is the point in the grid where we apply the force that will be causing the migration. The direction, θ, of the force is calculated in the tip cell, and is given by

$$\theta = \tan^{-1} \frac{V'_y}{V'_x},$$

where V'_y is the gradient of V in the vertical axis and V'_x the gradient of V in the horizontal axis. Now, the angle θ can be used in the rotational matrix to calculate $\bigtriangledown \cdot \mathbf{F}$ (2.18), which will be used to obtain χ. The method is the same as to calculate ω:

$$\chi(i,j)^{(n+1)} = \chi(i,j)^{(n)} + \frac{1}{4}[\chi(i+1,j)^{(n)} + \chi(i-1,j)^{(n)} + \chi(i,j+1)^{(n)} + \\ + \chi(i,j-1)^{(n)} - 4\chi(i,j)^{(n)} + \bigtriangledown \cdot \mathbf{F}(i,j)^{(n)}].$$

Because $\bigtriangledown^2 \omega = \frac{-\alpha\phi + \chi^t}{L_0}$, the calculation of ω must be updated to include χ:

$$\omega(i,j)^{(n+1)} = \omega(i,j)^{(n)} + \frac{1}{4}\left[\omega(i+1,j)^{(n)} + \omega(i-1,j)^{(n)} + \omega(i,j+1)^{(n)} + \right. \\ \left. + \omega(i,j-1)^{(n)} - 4\omega(i,j)^{(n)} - \frac{\alpha\phi(i,j)^{(n)} + \chi(i,j)^{(n)}}{L_0}\right].$$

As in the biological case, the tip cell must be moving. To approximate our model to reality, the position of the tip cell is changed after the force is applied during a certain number of iterations. Starting in the position of the actual tip cell, we follow the direction of migration searching for its new position in the sprout. Therefore, in each iteration, we move $\cos(\theta)$ in the horizontal, $\sin(\theta)$ in the vertical and calculate the weighted average of that point. We repeat this step until we find a value near zero or negative. If it's near zero, we have already found an interface point, thus the new position of the tip cell. If it's negative, it means we passed from the EC's phase domain to the ECM phase domain without finding an interface point. In that case, we use the bisection method until we find the new position of the tip cell.

To better understand the influence of the factors we are having into account in sprout creation, we started initializing ϕ with the form of a capillary. After choosing where to apply the force, migration can be seen in figures (3.6) and (3.7) with different directions. The value of the constants of the model is based, when possible, in the literature. This is discussed in the next chapter.

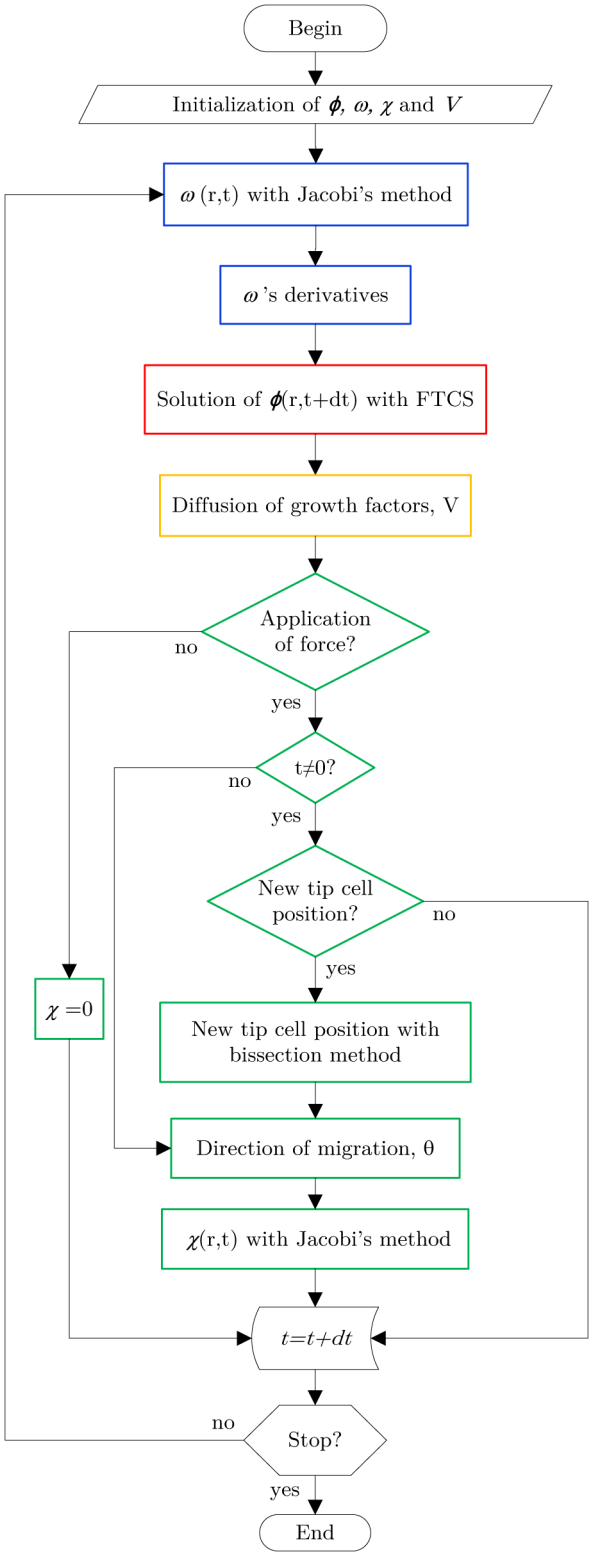

FIGURE 3.5: Flowchart for solving the Cahn-Hilliard equation with elastic properties, cell migration and chemotaxis. New value of w is dependent not only on ϕ but also on χ. After applying the diffusion equation for the growth factors (yellow) we can calculate χ for the first iteration, having in account the direction of migration calculated with the gradients in the tip cell. We apply the same χ during an interval of iterations which is followed by a cool-off period. After each cool-off period, we look for the new position of the tip cell. Last steps, related to cell migration, are represented in green.

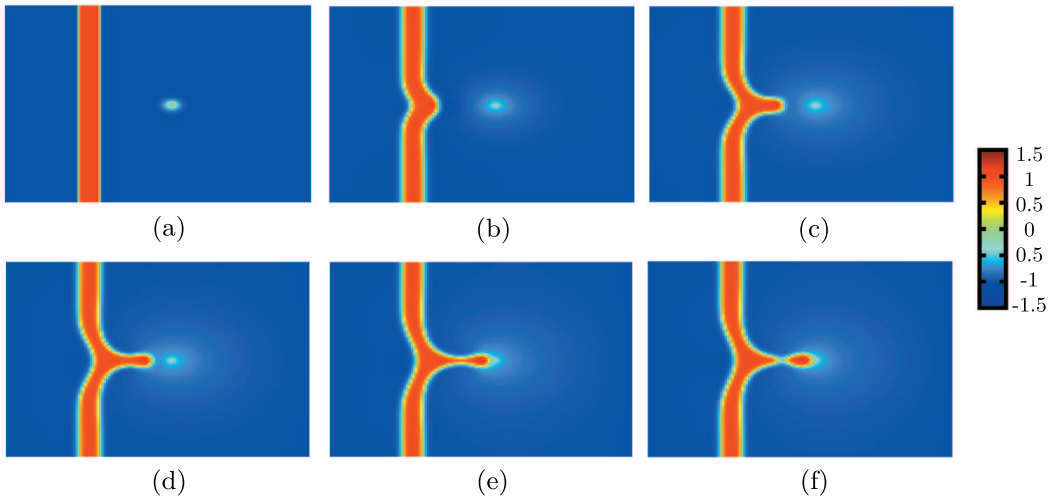

FIGURE 3.6: Simulation on a 130 by 130 lattice mesh of the evolution of ϕ with $A = 5$, $r = 5$, $L_0 = 1$, $\alpha = 0.13$, $D_g = 0.9$, $\alpha_c = 0.1$ and $\mu_1 = 0.13$, using the Cahn-Hilliard equation with elastic properties, cell migration and chemotaxis, for (a) 0; (b) 9000; (c) 29000; (d) 39000; (e) 49000; (f) 52000 iterations. In few iterations we can observe the creation of a sprout that grows in the direction of VEGF font (in light blue). Its easy to observe the occurrence of diffusion of VEGF from (a) to (b). In (f) the necessity of proliferation is evident: there's disruption of the developing sprout.

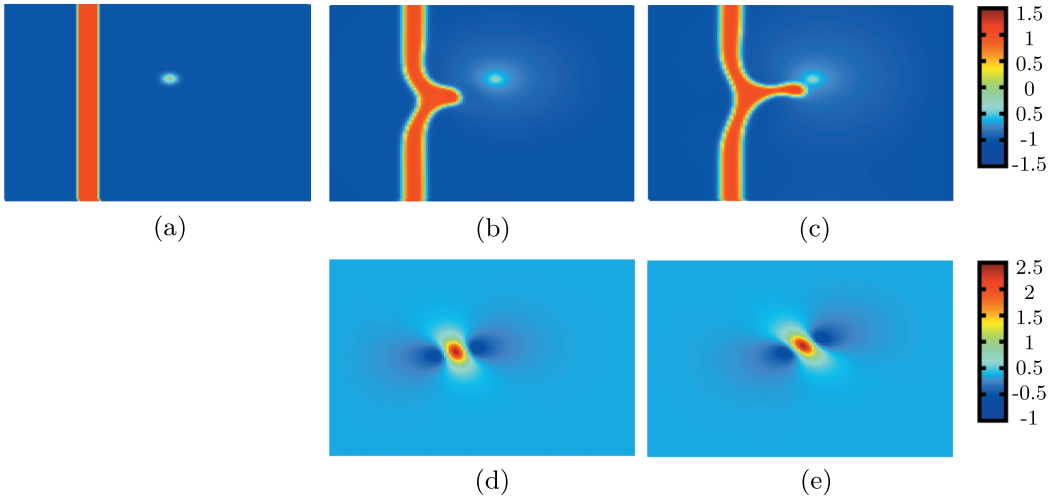

FIGURE 3.7: Repetition of the simulation in figure (3.7) with growing of the sprout in a different direction, for (a) 0; (b) and (d) 29000; (c) and (e) 54000 iterations. In (d) and (c) is represented χ, which is triggering movement in (b) and (c), respectively. We can observe the inclination of χ increasing from (d) to (e). This occurs because changes of VEGF's gradient in the vertical direction felt by the tip cell in (b) are less than when the tip cell gets closer to the font.

3.4 Proliferation

By adding the proliferation term (2.20) to the calculation of ϕ, even with little proliferation as can be seen on figure 3.9, we prevent possible disruption of early formed sprout (see figure 3.8). Despite we are considering proliferation in the simulation, disruption can still occur if we use small proliferation coefficients.

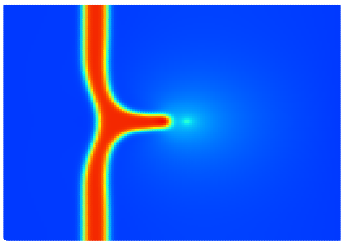

(a)

FIGURE 3.8: Simulation on a 130 by 130 lattice mesh of the evolution of ϕ with proliferation coefficient $k_V = 0.05$, for (a) 53000 iterations. New sprout doesn't have an abnormal form as before and the possibility of disruption is smaller.

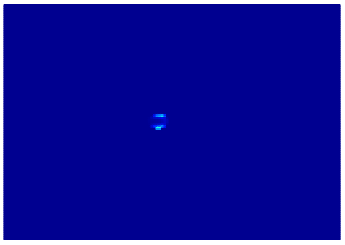

(a)

FIGURE 3.9: Proliferation sites (light blue) from figure 3.8, for (a) 53000 iterations. It occurs mainly in the stalk cell immediately before the tip cell.

Chapter 4

Exploring the model

In this chapter, we start by running the simulation with a greater/smaller value for parameters like intensity of the force applied, proliferation coefficients, among others. This way, we can study their individual influence in the overall system. For each case, we consider as a reference the figure 3.8. We maintained the same choice of values, except for the parameters in study. The better we know how the system behaves in response of each stimulus, the better we know how to control, improve and make it more robust.

After acquiring this knowledge, we study the system's behaviour in different situations, like the union of two sprouts. We expect the results can help us to better understand what happens in this type of phenomenons that often occur in the development of a vascular plexus.

4.1 Cell migration force

It was gathered from previous results of this model that by increasing the amplitude, F, the main difference was the increased velocity in which the pulling effect occurred[36].

After running the simulation with a more intense stimulus for cell migration, another difference was evident. Not only the velocity of growth was bigger but also the diameter of the sprout increased (see 4.1). Plus, the depression created in the main vessel on the left side is significantly bigger.

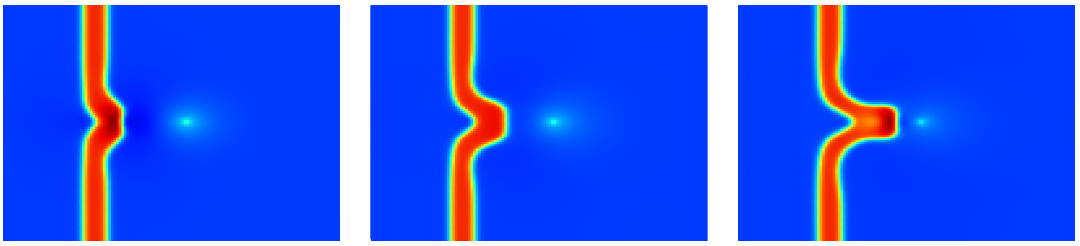

(a) (b) (c)

FIGURE 4.1: Greater cell migration force, $A = 15$, for (a) 5000; (b) 10000; (c) 15000 iterations. The dark spot seen in (a) and (c) is the consequence of applying χ. If A is excessive, disruption may occur in the place where χ is acting. Sprouting occurs faster, but there are differences in the morphology of the sprout and the main vessel.

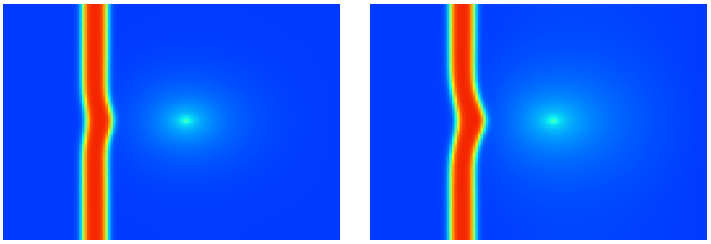

(a) (b)

FIGURE 4.2: Smaller cell migration force, $A = 1$, for (a) 20000; (b) 55000 iterations. From (a) to (b), almost any difference is noticed. This magnitude may be insufficient to trigger sprouting.

4.2 Proliferation

Being affected by VEGF and the force applied, there are many ways to alter proliferation.

The most obvious way to alter proliferation is by increasing the proliferation coefficient, k_V. In figure 4.3, it is observed that the sprout grew towards the VEGF font more quickly, as expected. Despite the difference is not significant, the sprout has a larger diameter. In the main vessel there is no noticeable change.

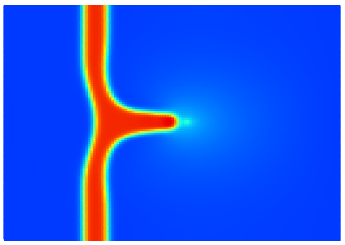

(a)

FIGURE 4.3: Greater proliferation coefficient, $k_V = 0.5$, for (a) 45000 iterations. It is observable a quicker growth and a greater sprout diameter.

In the other hand, the morphology is strongly compromised with the cut-off value considered in the Heaviside function, $\theta(\chi)$ (see figure 4.4). By decreasing its value, we say that we want proliferation to occur in a greater range of values, including the ones where very small values of χ are present (see figure 4.5). The consequence is a sprout with a triangular form.

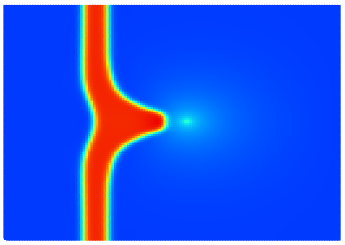

(a)

FIGURE 4.4: Absence of a cut-off value in $\theta(\chi)$, for (a) 31000 iterations. Sprout grows with a triangular form as a consequence.

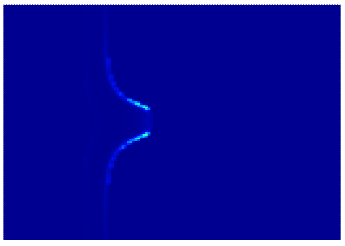

(a)

FIGURE 4.5: Proliferation sites (light blue) from figure 4.4, for (a) 31000 iterations. Proliferation occurs even in the main vessel. It is stronger near the tip cell.

4.3 Adhesion factor, α

The parameter α controls the adhesion force between the cells. This force is proportional to the $\bigtriangledown\phi$. If α is negative, a depression is caused in the main vessel instead of a sprout. The adhesion between cells forces the tissue to follow the leading cell. A superior value than the one used in 3.8, causes not only the tip cell but the material close to it to be dragged. In comparison with figure 3.6, the disruption was prevented (see figure 4.6). The material close to the tip cell was dragged more intensely.

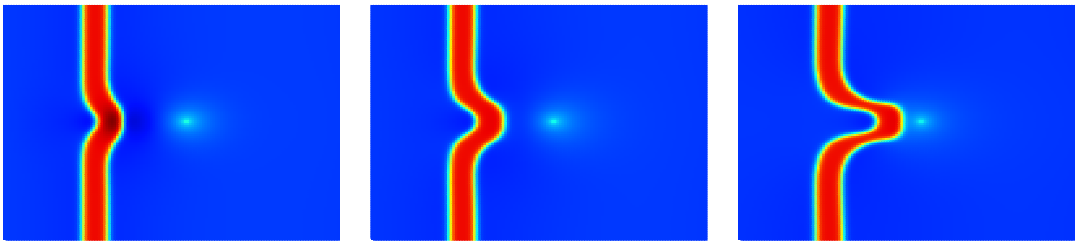

(a) (b) (c)

FIGURE 4.6: Greater adhesion factor, $\alpha = 1$, for (a) 5000; (b) 15000; (c) 25000 iterations. Proliferation was considered null ($k_V = 0$) and time step was decreased to half ($dt = 0.01$), in order to maintain convergence.

4.4 Regression

After a sprout grew horizontally in the direction of a VEGF font for some iterations, the location of the font and the tip cell was changed to another location. What we observed was the regression of the sprout portion where the tip cell was previously located (see figure 4.7).

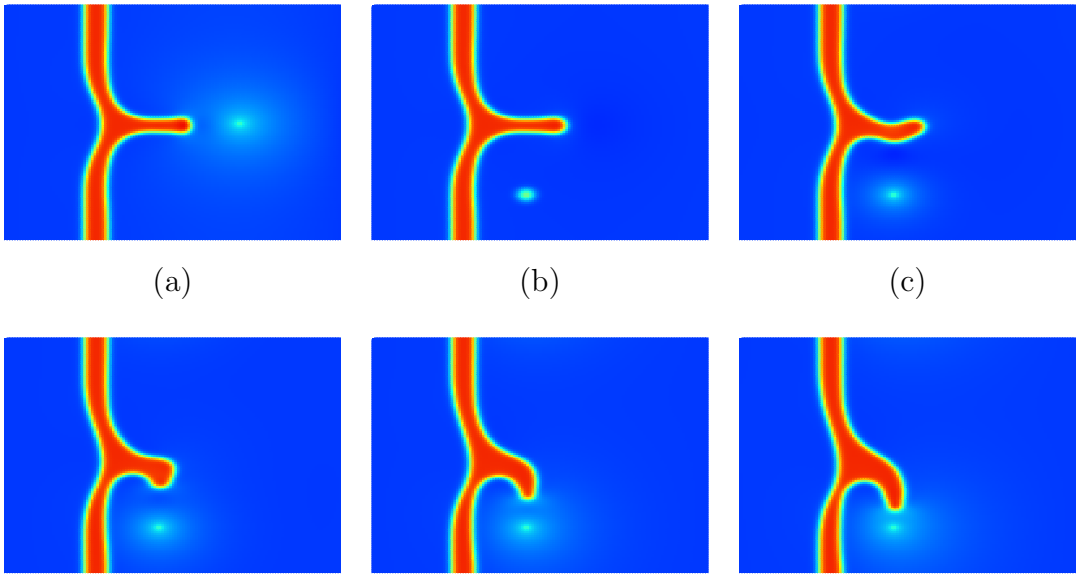

FIGURE 4.7: Regression of a sprout in favour of extension in another direction, for (a) 55000; (b) 60000; (c) 65000; (d) 75000; (e) 85000; (f) 95000 iterations. (a) The sprout grows horizontally in the direction of the VEGF gradient. (b) VEGF's font and tip cell position are changed. (c) and (d) Sprout's growth is redirected. (e) The part of the sprout where the tip cell was previously located has regressed completely. (f) The tip cell reaches the new VEGF font.

4.5 Anastomosis

Anastomosis is the formation of loops. It occurs after the sprout tips have migrated some distance into the ECM and branching as taken place. Tip cells fuse either with existing sprouts or with other tip cells. When two sprout tips fuse, a loop is closed and migration is stopped for both tip cells (see figure 4.8). When a sprout tip fuses with an existing sprout, a loop is closed and migration stops for the sprout tip[6].

We looked for ω, for the case of the figure 4.8. When this model was first applied, it was discovered that ω could help us predicting what would happen in the system[36]. That is what we show in the figure 4.9.

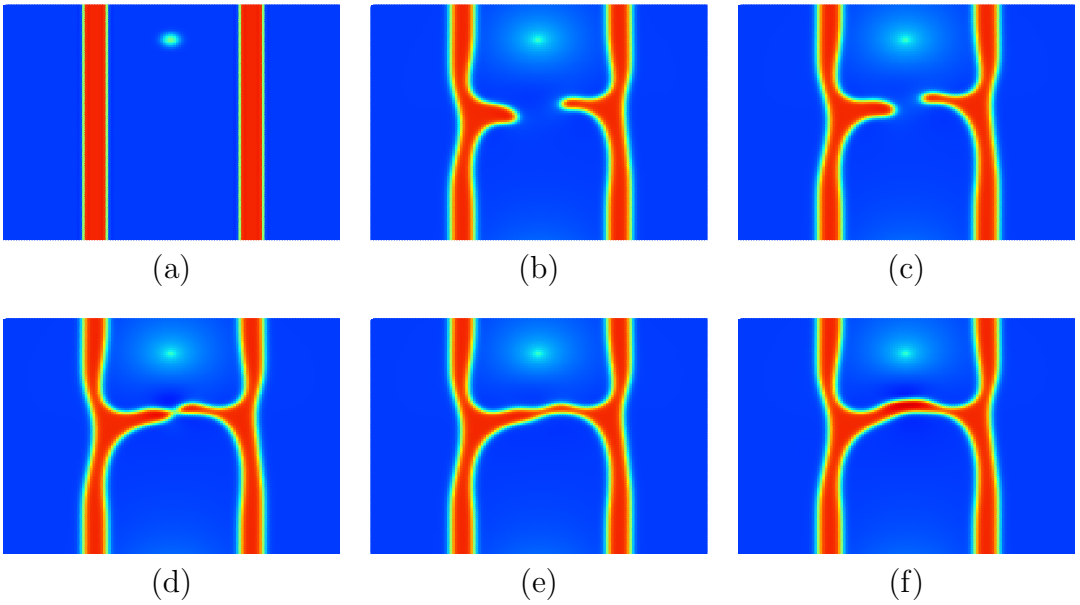

FIGURE 4.8: Fusion of two tip cells, for (a) 0; (b) 40000; (c) 50000; (d) 57000; (e) 58000; (f) 61000 iterations. A sprout was created in each main vessel. Both started growing in the direction of VEGF but the tip cells joined before they reached the font.

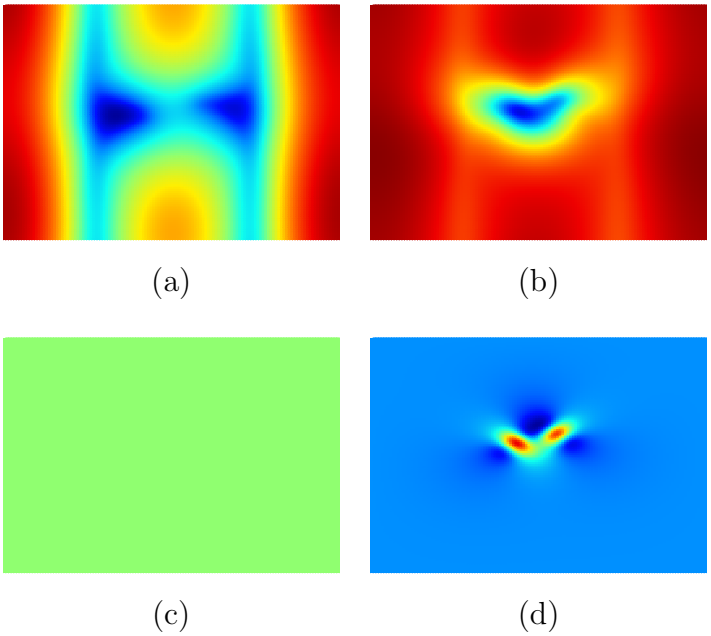

FIGURE 4.9: ω before the fusion of two tip cells, for (a) and (c) 40000; (b) and (d) 45000 iterations. ω functions as guidance for future work. Greater values are represented in dark blue and smaller values are represented in red. The regions with larger values of ω will be occupied by ϕ in some iterations. (a) ω during cool-off period. (b) ω during action of forces. (c) χ during cool-off period. (d) χ during the action of forces.

Looking at (b) in figure 4.9, we are able to predict in more than 10000 iterations before that sprouts are going to fuse. We can also notice the opposite signal of ω comparing with ϕ. Another important difference is the distribution and intensity of ω when we are in a cool-off period or not (when the tip cell force is not applied). During cool-off period, ω values are well distributed. They occur not only in the sprouts but also in the main vessels. Yet, its values are slightly bigger in the surrounding of the sprouts that are getting closer to each other. This may imply that there is an attraction force between portions of the same phase field. Plus, we can also observe that ω is more intense inside ϕ's phase field than in the interface. While forces are acting, ω is mainly concentrated in χ's field of action.

We realized that our model fails in other cases of anastomosis. Even with an increase in the parameters which influence positively proliferation, disruption occurs inevitably. This can be seen either in figures 4.10 and 4.11. We considered a notch inhibition of two cells in between the growing sprouts.

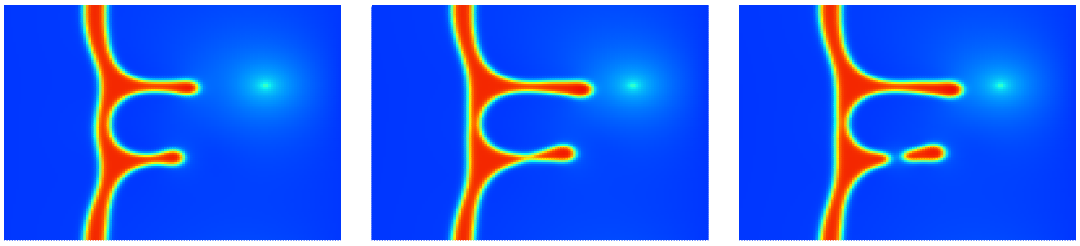

(a) (b) (c)

FIGURE 4.10: Double sprouting from the main vessel, for (a) 70000; (b) 90000; (c) 92000 iterations. Disruption of one of the sprouts. (a) Two sprouts grow from the main vessel. (b) The sprout further from the font starts disrupting. (c) The sprout further from the font disrupts.

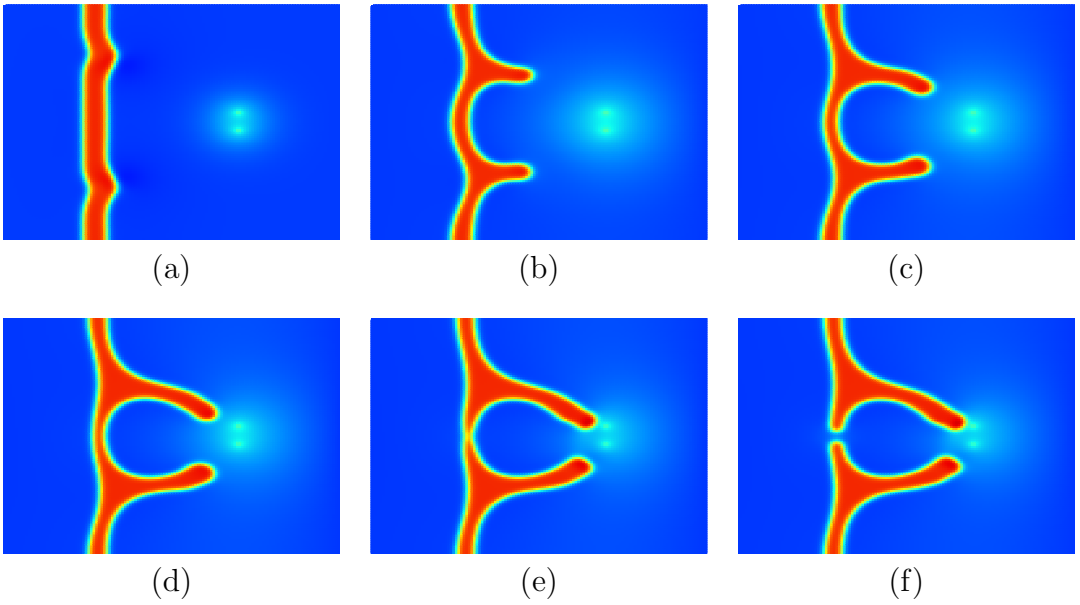

FIGURE 4.11: Double sprouting from the main vessel, for (a) 5000; (b) 50000; (c) 80000; (d) 100000; (e) 110000; (f) 113000 iterations. Disruption of the main vessel in (f).

Chapter 5

New proliferation approach

Our model's proliferation term is able to make a sprout grow straight but has some limitations. It happens only in interface. This is not close to reality and revealed to be inefficient when more than one sprout is growing.

The first step to make this new approach to proliferation was precisely to get it closer to reality. Hence, we jumped from considering proliferation individually in a point to consider proliferation in a cell. In practice, when calculating proliferation in a lattice point we have in consideration its neighbours. More specifically, it is the average proliferation of its neighbours. The neighbours considered are the ones placed inside a circle with the radius of the cell. To avoid proliferation in interface, we only go through points where ϕ is greater than 0.5.

Both chemotaxis and mechanical forces affect proliferation. Firstly, we will study them individually with this new approach. Secondly, we will look for the best combination between them.

It is important to highlight that all the results presented were obtained around iteration 30 000, unless the cases where results diverged due to exaggerated proliferation. Plus, when talking about conditions greater than zero, a small value of cut-off was always used.

Proportional with angiogenic factor concentration: Obviously, the first criteria to have proliferation here is the presence of VEGF. Proliferation varies directly with the quantity of VEGF until a maximum value of proliferation, P_{max} where the amount of VEGF is greater than a maximum value of VEGF, V_{max}, as shown in next figure.

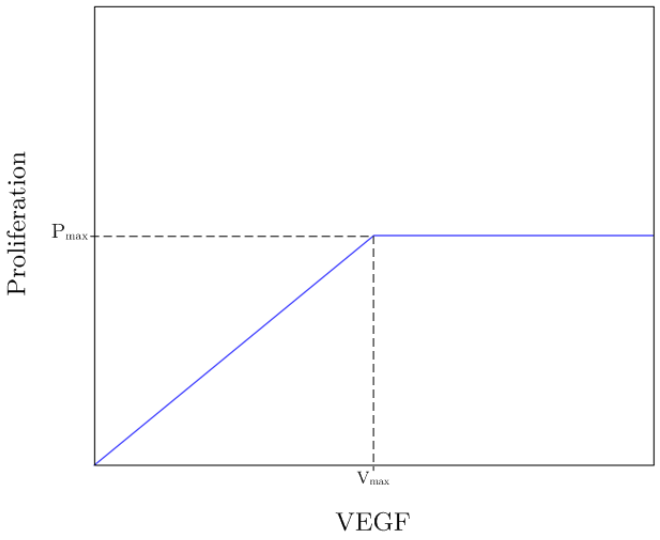

FIGURE 5.1: Relation of proliferation with the amount of VEGF sensed in a lattice point. The proliferation varies directly with VEGF until a maximum proliferation value, $Pmax$, is reached.

No doubts arise on the antagonistic influence of V_{max} and P_{max} in proliferation. While the first one is inversely proportional, the second one is directly proportional to the proliferation at a given concentration of VEGF, as can be seen in figure 5.2.

We observe that for low proliferation there is the possibility of disruption, while for very high proliferation also the main vessels increase their size. The range of parameters where the new vessel is well formed is small.

The disadvantage of this approach is the increase of main vessel's diameter. This is easily explained: there is VEGF consumed at the main vessel and we are considering proliferation where VEGF exists. Through literature, we know that small calibre vessels like this do not increase diameter.

Proportional with VEGF where mechanical force exists: To avoid the undesired result obtained before, we should select the places that are in distension. Considering the form of χ (see figure 2.4), this means that we want proliferation

to occur in locations of positive χ and where ϕ is also positive. Therefore, we add the condition

$$\chi^t(i,j) - \alpha(\phi(i,j) - 1) > 0.$$

This prevents the main vessel from enlarging. A small add-on like this, makes a great difference as can be seen in figure 5.3. Here, for small proliferation there is also disruption, but for large proliferations the new vessels are well formed without a thickening of the main vessel.

Proportional with mechanical force: We consider proportionality with mechanical force similar with the proportionality with VEGF. The only difference is that instead of a maximum value of VEGF, there is a maximum value of χ. It is an absolute value, because we want proliferation to happen on one of the positive regions of χ.

In figure 5.4, it is clear that this approach was unsuccessful. Abnormal vessels, in the form of a triangular shape, are created. It is difficult to find a combination of χ_{max} and P_{max} that can create an acceptable sprout.

Proportional with mechanical force where VEGF exists: This is obtained by adding the simple condition $V(i,j) > 0$.

The triangular form and the undesired proliferation in the left side of the main vessel were prevented in some cases, but the region of good vessel is very restrict.

Discussion

After solving the problem with the main vessel's dilatation, proliferation due to VEGF in places suffering distension seemed to be a good solution. When the proportionality is related to mechanical force, the values of proliferation used before revealed to be excessive. After decreasing its value, the triangularity form is still difficult to avoid. However, this effect is reduced when the condition to have the presence of VEGF is included. But its still difficult to make a sprout grow straight.

Surely, the combinations of the two boosters of proliferation (VEGF and distension) results better than when one of them is acting alone. A more detailed

study was made in order to understand which of the approaches was more robust (see figure 5.6).

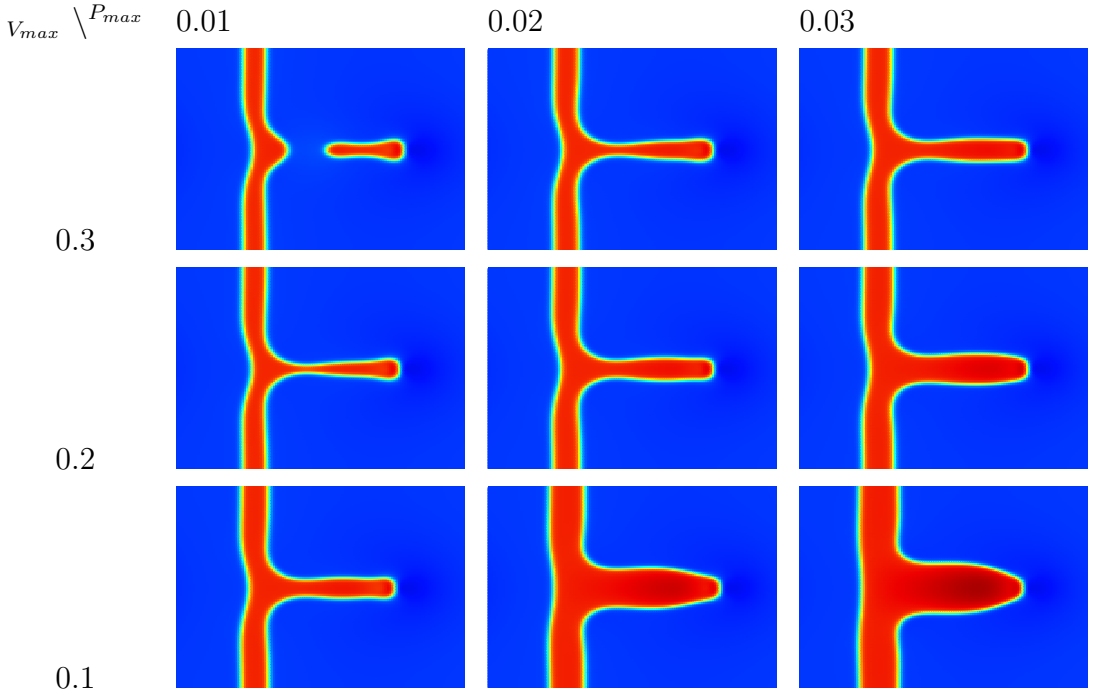

FIGURE 5.2: Results for proliferation proportional with VEGF. It is observed an undesired enlargement of the main vessel.

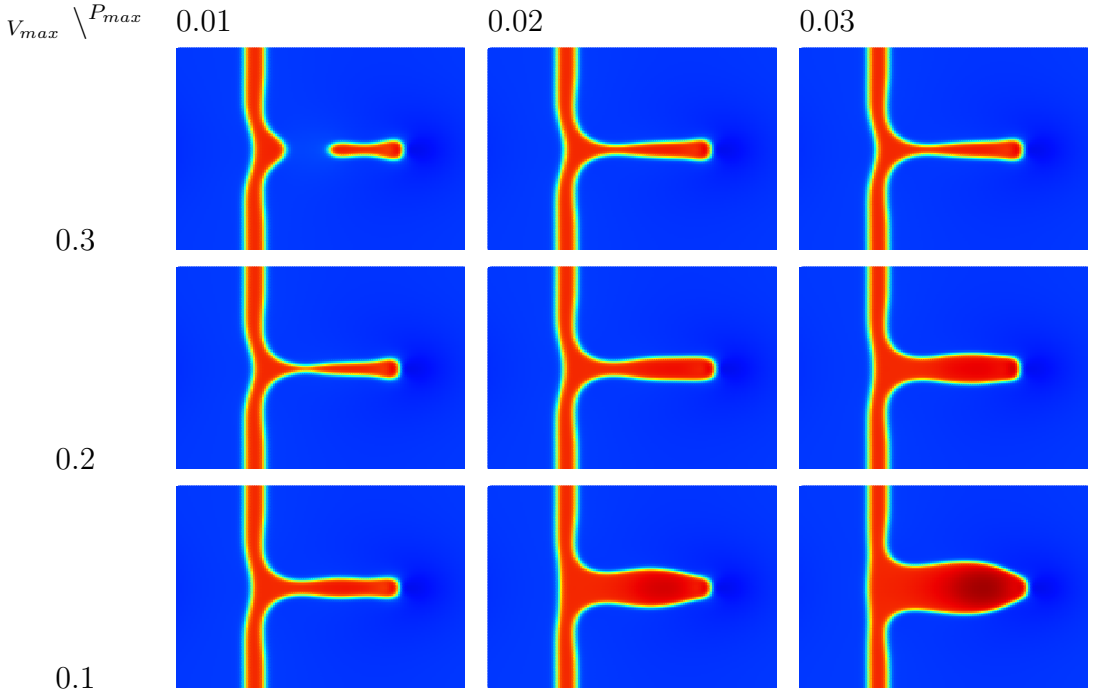

FIGURE 5.3: Results for proliferation proportional with VEGF only where mechanical force exists. Enlargement of the main vessel is prevented.

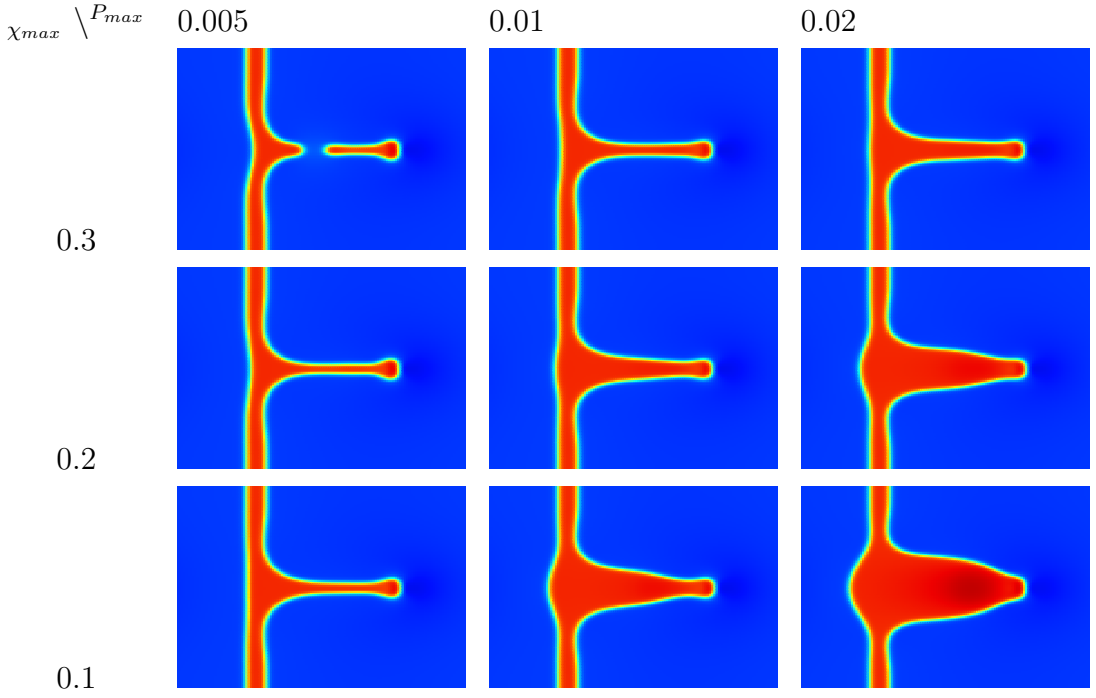

FIGURE 5.4: Results for proliferation proportional with mechanical force. It is observed the creation of triangular sprouts in most of the cases.

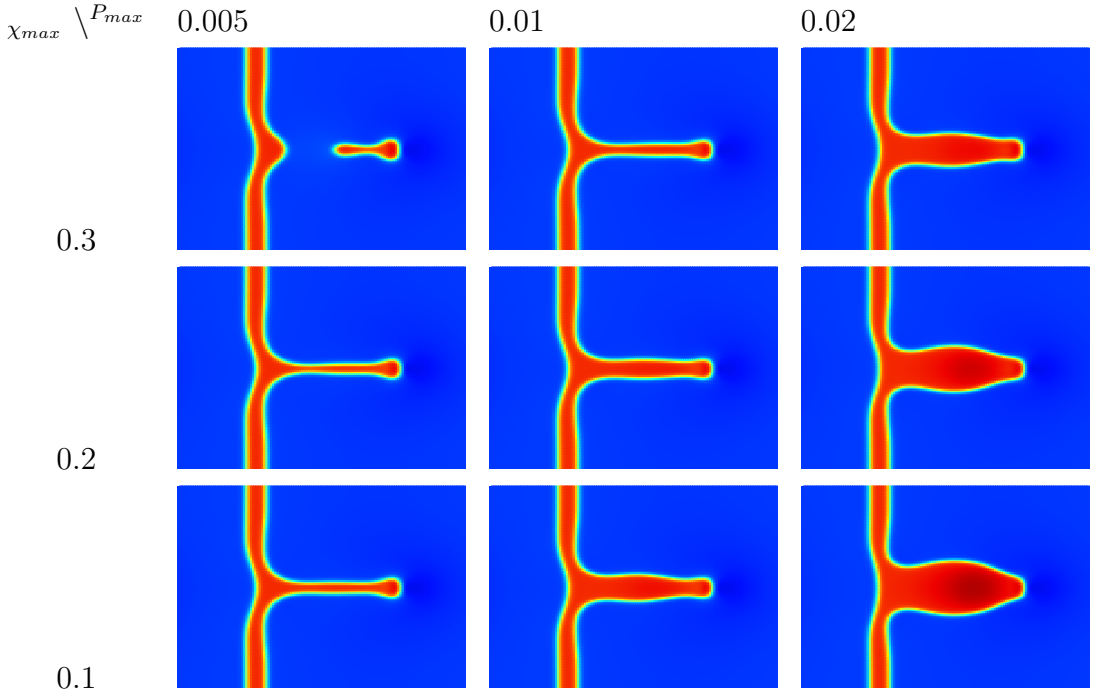

FIGURE 5.5: Results for proliferation proportional with mechanical force only where VEGF exists. Triangular sprouts are prevented but the vessels are not straight.

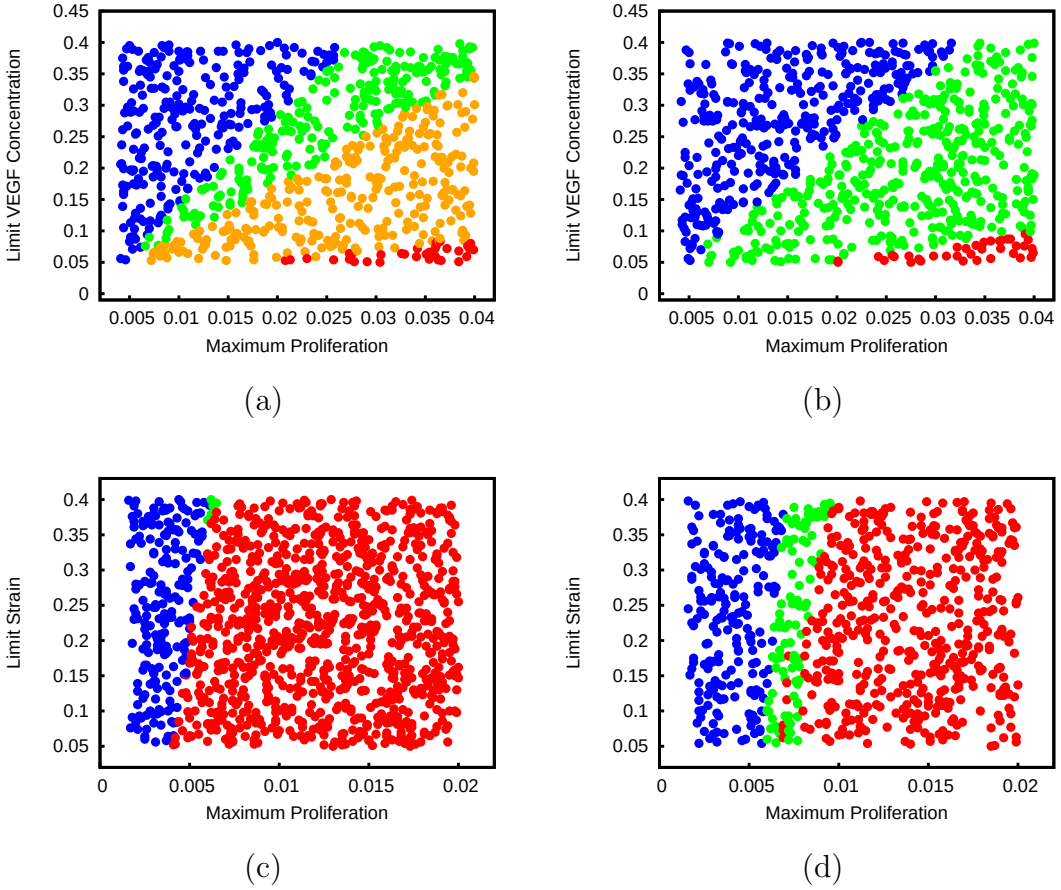

FIGURE 5.6: Detailed study of each proliferation's performance. The meanings of the colours are the following: blue for the sprouts that disrupted, green for the good sprouts, orange for the cases where the main vessel increased diameter and red for tortuous/triangular sprouts. (a) Proliferation proportional with VEGF. (b) Proliferation proportional with VEGF only where mechanical distension exist. (c) Proliferation proportional with mechanical force. (d) Proliferation proportional with mechanical force only where VEGF exists.

The better option revealed to be the one proportional to VEGF where mechanical force is acting. It was the one capable of creating good sprouts in the biggest range of values.

Trying again to create anastomosis, the improvement from the attempts in Chapter 4 can be observed in figure 5.7.

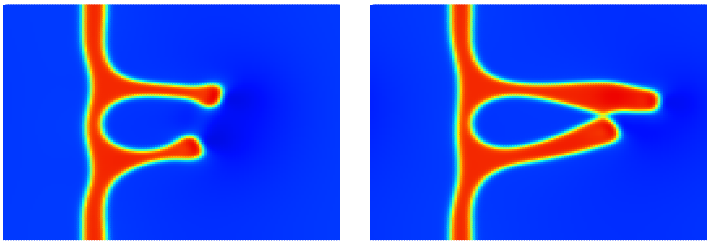

(a) (b)

FIGURE 5.7: New attempt to create an anastomosis with the new proliferation approach ($V_{max} = 0.2$ e $P_{max} = 0.03$), for (a) 20000; (b) 33000 iterations. Disruption does not occur.

Chapter 6

Conclusions and future work

Although we did not include blood pressure in the model as planned in the beginning of the year, important steps were made in increasing the robustness of the model. The first goal of this project was achieved with success. The parameters found on literature worked well in our simulation, hence providing a more concrete biological foothold for the model. Despite having still some constants with values chosen by estimation, being sure about the values tested allows the development of studies to obtain the correct values for the constants that remain unknown. We run the simulation over a large range of values for the proliferation, testing also different possible dependences for how the stalk cells proliferation depends on stress and VEGF concentration. These studies enabled us to choose the best dependence for the new proliferation approach. This method can be applied to other parameters of the simulation.

After this year, we understand better the influence of the constant α in the model. However, there are still doubts on how to obtain experimentally the value to assign to this effective adhesion. Moreover, the force's intermittency is another factor with influence in the final result. Its frequency should also be explored in the future. When both are understood, advances in the model can be made more comfortably. Besides including more mechanical and biological factors, a full angiogenesis model should also include a degree of stochasticity that is currently not present.

Our model is computationally heavier with the new proliferation approach. Before creating a full parallelized code, the possibility of optimizing it by applying implicit and higher order numerical methods should be considered.

This model can be validated by comparing its predictions with experimental results. This should be made for example, in terms of sprouting velocity.

A three dimensional version of this model can be implemented with few alterations. Most of the model's equations can describe angiogenesis in a three dimensional environment by changing the dimension parameter d. Adapting the search algorithm for the tip cell is what requires larger programming efforts.

The implementation of this algorithm is very complex. Whereas it requires a lot of effort and time to improve, it is undoubtedly important to further our understanding of the mechanic influences in angiogenesis and provide analogy close to the real case.

Models for angiogenesis that include mechanical effects are able to explore new treatments for diseases related to this biological process. Until now, treatments were proposed based on chemical methods. Understanding how ECs migrate in tissues with different stiffness may give new insights based on mechanical effects, on how to normalize pathological vasculatures. This type of modelling coupled to experimental validation helps to understand better how angiogenesis proceeds in the complex in vivo environment, providing new clues on how to act upon this complex process that is determinant for the development of many pathologies.

Appendix A

Functional derivative of free energy, F (2.2)

In a functional derivative, instead of differentiating a function with respect to a variable, one differentiates a functional with respect to a function. We want to reach the following form in order to get the $\frac{\delta F}{\delta \phi}$ expression:

$$\delta F = \int \frac{\delta F}{\delta \phi} \delta\phi \; d\mathbf{r}$$

To do that, we start by calculating $F[\phi + \delta\phi]$:

$$\begin{aligned} F[\phi+\delta\phi] &= \int \left[\frac{(\phi+\delta\phi)^4}{4} - \left(\frac{\phi+\delta\phi}{2}\right)^2 + \frac{\epsilon^2}{2}\nabla(\phi+\delta\phi)^2 \right] d\mathbf{r} \\ &= \int \left[\frac{\phi^4 + 4\phi^3\delta\phi + 16\phi^2\delta\phi^2 + 4\phi\delta\phi^3 + \delta\phi^4}{4} - \frac{\phi^2 + 2\phi\delta\phi + \delta\phi^2}{2} + \right. \\ &\qquad \left. + \frac{\epsilon^2}{2}\left[(\nabla\phi)^2 + 2\nabla\phi\cdot\nabla\delta\phi + (\nabla\delta\phi)^2\right] \right] d\mathbf{r} \end{aligned}$$

we then eliminate the $\delta\phi$ terms of higher order than 2, because of their approximation to zero:

$$= \underbrace{\int \left(\frac{\phi^4}{4} - \frac{\phi^2}{2} + \frac{\epsilon^2}{2}(\nabla\phi)^2 \right) d\mathbf{r}}_{F[\phi]} + \underbrace{\int \left(\phi^3\delta\phi - \phi\delta\phi + \epsilon^2\nabla\phi\nabla\delta\phi \right) d\mathbf{r}}_{\delta F}$$

after integrating by parts with periodic boundary conditions the last term:

$$\delta F = \int \left(\phi^3 - \phi\right) \delta\phi \; d\mathbf{r} - \epsilon^2 \int \nabla^2\phi\delta\phi \; d\mathbf{r}$$

$$\frac{\delta F}{\delta \phi} = -\phi + \phi^3 - \epsilon^2\nabla^2\phi$$

Appendix B

Functional derivative of elastic force, F^{el}

Just like in A, we will calculate $\frac{\delta F^{el}}{\delta \mathbf{u}}$ starting from adding an increment to the function $\mathbf{u}$ from which F^{el} depends on.

$$F^{el}(\mathbf{u}+\delta\mathbf{u}) = F^{el}(\mathbf{u}) + \delta F^{el}(\mathbf{u},\delta\mathbf{u})$$

$$\begin{aligned} F^{el}(\mathbf{u}+\delta\mathbf{u}) &= \int \frac{1}{2}\left[\left(K-\frac{2\mu}{d}\right)(\partial_i(u_i+\delta u_i))^2 + \mu(\partial_i(u_j+\delta u_j)\cdot\partial_i(u_j+\delta u_j) + \right. \\ &\qquad \left. + \partial_i(u_j+\delta u_j)\cdot\partial_j(u_i+\delta u_i))\right]\ d\mathbf{r} \\ &= \int \frac{1}{2}\left[\left(K-\frac{2\mu}{d}\right)((\partial_i u_i)^2 + 2\partial_i u_i\partial_i\delta u_i) + \mu(\partial_i u_j\partial_i u_j + 2\partial_j u_i\partial_j\delta u_i + \right. \\ &\qquad \left. + \partial_i u_j\partial_j u_i + \partial_i\delta u_j\partial_j u_i + \partial_i u_j\partial_j\delta u_i)\right]\ d\mathbf{r} \end{aligned}$$

$$\begin{aligned} \delta F^{el}(\mathbf{u},\delta\mathbf{u}) &= \int \left[\left(K-\frac{2\mu}{d}\right)\partial_k u_k\partial_i\delta u_i + \mu(\partial_j u_i\partial_j\delta u_i + \partial_i u_j\partial_j\delta u_i)\right]\ d\mathbf{r} \\ &= \int \left[\left(K-\frac{2\mu}{d}\right)\partial_k u_k\delta_{ij} + \mu(\partial_j u_i + \partial_i u_j)\right]\partial_j\delta u_i\ d\mathbf{r} \\ &= \int \partial_j\sigma_{ij}\delta u_i\ d\mathbf{r} = -\int \partial_{ij}\sigma_j\delta u_i\ d\mathbf{r} \\ \frac{\delta F^{el}}{\delta\mathbf{u}} &= -\partial_j\sigma_{ij} \end{aligned}$$

Appendix C

Deduction of elastic energies

Consider $\mathbf{u} = \mathbf{u}^0 + \mathbf{u}^1$

Order $\mathbf{u}^0$

$$F_{el}{}^0 = \int \left[\frac{1}{2} \left(K - \frac{2\mu_0}{d} \right) \partial_i u_j^0 \partial_j u_j^0 + \frac{\mu_0}{2} (\partial_i u_j^0 \partial_i u_j^0 + \partial_i u_j^0 \partial_j u_i^0) - \chi \partial_i u_i^0 \right] \, d\mathbf{r}$$

$$\begin{aligned} F_{el}{}^0[u^0 + \delta u^0] = \int \Bigg[& \frac{1}{2} \left(K - \frac{2\mu_0}{d} \right) (\partial_i u_i^0 + \partial_i \delta u_i^0)(\partial_j u_j^0 + \partial_j \delta u_j^0) + \\ & + \frac{\mu_0}{2} ((\partial_i u_j^0 + \partial_i \delta u_j^0)(\partial_i u_j^0 + \partial_i \delta u_j^0) + ((\partial_i u_j^0 + \partial_i \delta u_j^0)(\partial_i u_i^0 + \partial_j \delta u_i^0)) + \\ & - \chi (\partial_i u_i^0 + \partial_i \delta u_i^0) \Big] \, d\mathbf{r} \end{aligned}$$

$$\begin{aligned} \delta F_{el}{}^0 &= \int \Bigg[\frac{1}{2} \left(K - \frac{2\mu_0}{d} \right) (\partial_i u_i^0 \partial_j \delta u_j^0 + \partial_i \delta u_i^0 \partial_j u_j^0) + \\ &\quad + \frac{\mu_0}{2} ((\partial_i u_j^0 \partial_i \delta u_j^0 + \partial_i \delta u_j^0 \partial_i u_j^0) + (\partial_i u_j^0 \partial_j \delta u_i^0 + \partial_i \delta u_j^0 \partial_j u_i^0)) + \\ &\quad - \chi \partial_i \delta u_i^0 \Big] \, d\mathbf{r} \\ &= \int \Bigg[\left(K - \frac{2\mu_0}{d} \right) \partial_i u_i^0 \partial_j \delta u_j^0 + \mu_0 (\partial_i u_j^0 \partial_i \delta u_j^0 + \partial_i u_j^0 \partial_j \delta u_i^0) + \\ &\quad - \chi \partial_i \delta u_i^0 \Big] \, d\mathbf{r} \end{aligned}$$

Integrating by parts:

$$
\begin{aligned}
&= \int \left[\left(K - \frac{2\mu_0}{d} \right) (-\partial_{ij} u_i^0) \delta u_j^0 + \mu_0 (-\partial_{ii} u_j^0 \delta u_j^0 - \partial_{ij} u_j^0 \delta u_i^0) + \partial_i \chi \delta u_i^0 \right] \\
&= \int \underbrace{\left[- \left(K - \frac{2\mu_0}{d} + \mu_0 \right) (\partial_{ji} u_j^0) - \mu_0 \partial_{jj} u_i^0 + \partial_i \chi \right]}_{\frac{\delta {F_{el}}^0}{\delta u_i^0}} \delta u_i^0 \; d\mathbf{r}
\end{aligned}
$$

Although we have reached an expression for $\frac{\delta {F_{el}}^0}{\delta u_i}$ we will simplify it in order to be easier to simulate it computationally:

$\mathbf{u}^0 = \nabla \omega$

$u_i^0 = \partial_i \omega$

$$
\begin{aligned}
\frac{\delta F_{el}^0}{\delta u_i} &= - \left(K - \frac{2\mu_0}{d} + \mu_0 \right) (\partial_{ji} u_j^0) - \mu_0 \partial_{jj} u_i^0 + \partial_i \chi \\
&= - \left(K - \frac{2\mu_0}{d} + \mu_0 \right) (\partial_{ijj} \omega) - \mu_0 \partial_{ijj} \omega + \partial_i \chi \\
&= - \left(K - \frac{2\mu_0}{d} + 2\mu_0 \right) (\partial_{ijj} \omega) + \partial_i \chi \\
&= 0
\end{aligned}
$$

Therefore:

$$
\partial_i \left[- \left(K - \frac{2\mu_0}{d} + 2\mu_0 \right) (\partial_{jj} \omega) + \chi \right] = 0
$$

which implies

$$
\nabla^2 \omega = \frac{\chi}{K - \frac{2\mu_0}{d} + 2\mu_0}. \tag{C.1}
$$

Now, we can write a simpler equation for ${F_{el}}^0$ using C.1:

$$
\begin{aligned}
{F_{el}}^0 &= \int \left[\left(K - \frac{2\mu_0}{d} \right) \frac{1}{2} \partial_{ii} \omega \partial_{jj} \omega + \frac{\mu_0}{2} (\partial_{ij} \omega \partial_{ij} \omega + \partial_{ij} \omega \partial_{ji} \omega) + \partial_i \chi \partial_i \omega \right] \; d\mathbf{r} \\
&= \int \left[\frac{1}{2} \left(K - \frac{2\mu_0}{d} + 2\mu_0 \right) \partial_{ii} \omega \partial_{jj} \omega - \chi \partial_{ii} \omega \right] \; d\mathbf{r} \\
&= \int \left[-\frac{1}{2} \left(K - \frac{2\mu_0}{d} + 2\mu_0 \right) \partial_{ii} \omega \partial_{jj} \omega \right] \; d\mathbf{r} \\
&= \int \frac{-\chi^2}{2 \left(K - \frac{2\mu_0}{d} + 2\mu_0 \right)} \; d\mathbf{r}
\end{aligned}
$$

Order u^1

$$
\begin{aligned}
{F_{el}}^1 = \int \Bigg[& \frac{1}{2}\left(\left(\frac{2(\mu_1\phi)}{d}\right)\partial_i u_i^0 \partial_j^0 u_j^0 + \left(K - \frac{2\mu_0}{d}\right)\partial_i u_i^1 \partial_j u_j^0 + \left(K - \frac{2\mu_0}{d}\right)\partial_i u_i^0 \partial_j u_j^1\right) - \\
& - \frac{\mu_1\phi}{2}(\partial_i u_j^0 \partial_i u_j^0 + \partial_i u_j^0 \partial_j u_i^0) + \frac{\mu_0}{2}(\partial_i u_j^1 \partial_i u_j^0 + \partial_i u_j^0 \partial_i u_j^1 + \partial_i u_j^1 \partial_j u_i^0 + \partial_i u_j^0 \partial_j u_i^1) + \\
& - \chi \partial_i u_i^1 \Bigg] \; d\mathbf{r} \\
= \int \Bigg[& \frac{\mu_1\phi}{d}\partial_{ii}\omega\partial_{jj}\omega + \left(K - \frac{2\mu_0}{d}\right)\partial_{jj}\omega\partial_i u_i^1 + 2\mu_0\partial_{ij}\omega\partial_i u_j^1 - \mu_1\phi\partial_{ij}\omega\partial_{ij}\omega + \partial_i\chi \cdot u_i^1 \Bigg] \; d\mathbf{r} \\
= \int \Bigg[& \frac{\mu_1\phi}{d}\partial_{ii}\omega\partial_{jj}\omega - \mu_1\phi\partial_{ij}\omega\partial_{ij}\omega - \left(K - \frac{2\mu_0}{d}\right)(\partial_{ijj}\omega)u_i^1 - 2\mu_0\partial_{iij}\omega u_j^1 + \partial_i\chi \cdot u_i^1 \Bigg] \; d\mathbf{r} \\
= \int \Bigg[& \frac{\mu_1\phi}{d}\partial_{ii}\omega\partial_{jj}\omega - \mu_1\phi\partial_{ij}\omega\partial_{ij}\omega + \left(-\left(K - \frac{2\mu_0}{d} + 2\mu_0\right)\partial_{ijj}\omega + \partial_i\chi\right)u_i^1 \Bigg] \; d\mathbf{r} \\
= \int \Bigg[& \frac{\mu_1\phi}{d}\partial_{ii}\omega\partial_{jj}\omega - \mu_1\phi\partial_{ij}\omega\partial_{ij}\omega \Bigg] \; d\mathbf{r}
\end{aligned}
$$

Appendix D

Functional derivative of free energy with elastic force, F (2.16)

Considering the simplifications,

$$\chi = -\alpha\phi + \chi^t$$

and

$$\partial_{ii}\omega = \frac{\chi}{K - \frac{2\mu_0}{d} + 2\mu_0} = \frac{\chi}{L_0},$$

we can write $F + \delta F = F\left[\phi + \delta\phi\right]$ as:

$$\begin{aligned} F\left[\phi+\delta\phi\right] = \int \Bigg[& \frac{(\phi+\delta\phi)^4}{4} - \frac{(\phi+\delta\phi)^2}{4} + \frac{\varepsilon^2}{2}(\bigtriangledown(\phi+\delta\phi))^2 - \frac{(-\alpha(\phi+\delta\phi)+\chi^t)^2}{2L_0} + \\ & + \mu(\phi+\delta\phi)\left(\partial_{ii}(\omega+\delta\omega)\partial_{jj}(\omega+\delta\omega) - \partial_{ij}(\omega+\delta\omega)\partial_{ij}(\omega+\delta\omega)\right)\Bigg]\ d\mathbf{r} \\ = \int \Bigg[& \left(\frac{\phi^4}{4} - \frac{\phi^2}{4} + \frac{\varepsilon^2}{2}(\bigtriangledown\phi)^2\right) + \left(\frac{4\phi^3\delta\phi}{4} - \phi\delta\phi + \frac{2\varepsilon^2 \bigtriangledown\phi \bigtriangledown\delta\phi}{2}\right) - \\ & - \frac{(-\alpha\phi+\chi^t)^2}{2L_0} - \frac{2\delta\phi(-\alpha\phi+\chi^t)(-\alpha)}{2L_0} + \mu_1\phi(\frac{1}{d}\partial_{ii}\omega\partial_{jj}\omega - \partial_{ij}\omega\partial_{ij}\omega) + \\ & + \mu_1\delta\phi(\frac{1}{d}\partial_{ii}\omega\partial_{jj}\omega - \partial_{ij}\omega\partial_{ij}\omega) + \\ & + \mu_1\phi\left(\frac{2}{d}\partial_{ii}\omega\left(-\frac{\alpha}{L_0}\delta\phi\right) + 2\partial_{ij}\omega\partial_{ij}\left[\frac{-1}{\partial_{kk}}\frac{\alpha}{L_0}\delta\phi\right]\right)\Bigg]\ d\mathbf{r} \end{aligned}$$

$$\begin{aligned}\delta F = \int \Bigg[& (-\phi + \phi^3)\delta\phi + \varepsilon^2 \bigtriangledown \phi \cdot \bigtriangledown \delta\phi + \frac{\alpha}{L_0}(-\alpha\phi + \chi^t)\delta\phi + \\ & + \mu_1 (\frac{1}{d}\partial_{ii}\omega\partial_{jj}\omega - \partial_{ij}\omega\partial_{ij}\omega)\delta\phi + \\ & + \mu_1\phi \left(\frac{-2}{d}\partial_{ii}\omega\frac{\alpha}{L_0}\delta\phi + \frac{2\alpha}{L_0}\partial_{ij}\omega\partial_{ij}\left[\frac{1}{\partial_{kk}}\delta\phi\right]\right)\Bigg]\ d\mathbf{r} \\ = \int \Bigg[& -\phi + \phi^3 - \varepsilon^2 \bigtriangledown^2 \phi - \frac{\alpha^2}{L_0}\phi + \frac{\alpha\chi^t}{L_0} + \\ & + \mu_1 (\frac{1}{d}\partial_{ii}\omega\partial_{jj}\omega - \partial_{ij}\omega\partial_{ij}\omega) - \\ & - \mu_1\phi\frac{2\alpha}{L_0 d}\partial_{ij}\omega + \mu_1\frac{2\alpha}{L_0\partial_{kk}}\partial_{ij}\left[\phi\partial_{ij}\omega\right]\Bigg]\delta\phi\ d\mathbf{r}\end{aligned}$$

We reached an expression for $\frac{\delta F}{\delta\phi}$ which can be further simplified to:

$$\frac{\delta F}{\delta\phi} = -\phi + \phi^3 - \varepsilon^2 \bigtriangledown \phi - \frac{\alpha\chi}{L_0} + \mu_1(\partial_{ij}\omega\partial_{ij}\omega - \frac{1}{d}(\bigtriangledown^2\omega)^2) - 2\frac{\mu_1\alpha}{L_0}\left(\frac{\phi}{d}\partial_{ii}\omega + \frac{1}{\partial_{kk}}\partial_{ij}\left(\phi\partial_{ij}\omega\right)\right)$$

Bibliography

[1] Akira Onuki. *Phase Transition Dynamics*. Cambridge University Press, Cambridge, p.566-576, 2004.

[2] A. S. Azmi. *Systems Biology in Cancer Research and Drug Discovery*. Springer, Dordrecht, p.199-220, 2012.

[3] P. Carmeliet and R. K. Jain. Angiogenesis in cancer and other diseases. *Nature*, 407:249–257, September 2000.

[4] T. H. Adair and J. P. Montani. *Angiogenesis*. Morgan & Claypool Life Sciences, San Rafael (CA), Chapter 1-Overview of Angiogenesis, 2010.

[5] D. J. Hicklin and L. M. Ellis. Role of the vascular endothelial growth factor pathway in tumor growth and angiogenesis. *J Clin Oncol*, 23(5):1011–1027, 2005.

[6] F. Milde, M. Bergdorf, and P. Koumoutsakos. A hybrid model for three-dimensional simulations of sprouting angiogenesis. *Biophysical Journal*, 95 (368):3146–3160, October 2008.

[7] P. Koumoutsakos, I. Pivkin, and F. Milde. The fluid mechanics of cancer and its therapy. *Annual review of fluid mechanics*, 45:325–355, October 2012. URL `http://minerva.ufpel.edu.br/~alejandro.martins/dis/2013_2/mecflu/web/material/artigos/annurev-fluid-120710-101102.pdf`.

[8] K. Bentley, G. Marriggi, and H. Gerart. The shunt problem: control of functional shunting in normal and tumour vasculature. *Nat Rev Cancer*,

8(10):587–593, August 2010. URL http://www.ncbi.nlm.nih.gov/pmc/articles/PMC3109666/.

[9] R. K. Jain. Normalization of tumor vasculature: an emerging concept in antiangiogenic therapy. *Science*, 307:58–62, 2005.

[10] K. A. Rejniak and A. R. A. Anderson. Hybrid models of tumor growth. *Wiley Interdiscip Rev Syst Biol Med.*, 3(1):115–125, Jan-Fev 2011. URL http://www.ncbi.nlm.nih.gov/pmc/articles/PMC3057876/.

[11] M. Silberman, Y. D. Barac, H. Yahav, E. Wolfovitz, S. Einav, N. Resnick, and O. Binah. Shear stress-induced transcriptional regulation via hybrid promoters as a potential tool for promoting angiogenesis. *Angiogenesis*, 12: 231–242, 2009.

[12] P. Carmeliet. Angiogenesis in life, disease and medicine. *Nature*, 438:932–936, December 2005. URL http://web.mit.edu/hst527/www/readings/Lecture%2013/Carmeliet-Angiog-Review-2005%20.pdf.

[13] I. Buschmann and W. Schaper. Arteriogenesis versus angiogenesis: Two mechanisms of vessel growth. *Physiology*, 14(3):121–125, June 1999. URL http://physiologyonline.physiology.org/content/14/3/121.

[14] A. Das, D. Lauffenburger, H. Asada, and R. D. Kamm. A hybrid continuum-discrete modelling approach to predict and control angiogenesis: analusis of combinatorial growth factor and matrix effects on vessel-sprouting morphology. *Phil. Trans. R. Soc. A*, 368(8):2937–2960, May 2010.

[15] M. J. C. Hendrix, E. A. Seftor, A. R. Hess, and R. E. B. Seftor. Vasculogenic mimicry and tumour-cell plasticity: lessons from melanoma. *Nature Reviews Cancer*, 3(3):411–421, June 2003. URL http://physiologyonline.physiology.org/content/14/3/121.

[16] G. Liu, A. A. Qutub, P. Vempati, F. M. Gabhann, and A. S. Popel. Module-based multiscale simulation of angiogenesis in skeletal muscle. *Theoretical*

Biology and Medical Modelling, 8, April 2011. URL http://www.tbiomed.com/content/8/1/6.

[17] J. Folkman. Angiogenesis in cancer, vascular, rheumatoid and other disease. *Nat Med)*, 1(1):27–31, May 1995.

[18] J. W. Sang and L. L. Munn. Fluid forces control endothelial sprouting. *PNAS*, 108(37):15342–15347, 2011. URL http://www.pnas.org/content/108/37/15342.

[19] M. A. Konerding, A. Turhan, and S. J. Mentzer. Inflammation-induced intussusceptive angiogenesis in murine colitis. *Anat Rec (Hoboken)*, 438(5): 849–857, May 2010. URL http://www.ncbi.nlm.nih.gov/pmc/articles/PMC3045768/.

[20] S. J. Mentzer and M. A. Konerding. Intussusceptive angiogenesis: expansion and remodeling of microvascular networks. *Angiogenesis*, 17:499–509, 2014. URL http://www.ncbi.nlm.nih.gov/pubmed/24668225.

[21] G. S. Marchand, N. Noiseux, J. F. Tanguay, and M. G. Sirois. Blockade of in vivo vegf-mediated angiogenesis by antisense gene therapy: role of flk-1 and flt-1 receptors. *American Journal of Physiology - Heart and Circulatory Physiology*, 282:294–204, January 2002. URL http://ajpheart.physiology.org/content/282/1/H194.

[22] S. P. Herbert, J. Y. Cheung, and D. Y. Stainier. Determination of endothelial stalk versus tip cell potential during angiogenesis by h2.0-like homeobox-1. *Curr Biol.*, 19(22):1789–94, October 2012. URL http://www.ncbi.nlm.nih.gov/pubmed/22921365.

[23] L.K. Phng and Holger Gerhardt. Angiogenesis: A team effort coordinated by notch. *Developmental Cell*, 2(16):196–208, February 2009. URL http://www.sciencedirect.com/science/article/pii/S1534580709000434.

[24] X. Zheng, G.Y. Koh, and T. Jackson. A continuous model of angiogenesis: Initiation, extension, and maturation of new blood vessels modulated

by vascular endothelial growth factor, angiopoietins, platelet-derived growth factor-b, and pericytes. *Discrete and Continuous Dynamical Systems - Series B*, 18(4):1109 – 1154, June 2013. URL `https://www.aimsciences.org/journals/displayArticlesnew.jsp?paperID=8279`.

[25] M. J. Plank, B. D. Sleeman, and P. F. Jones. A mathematical model of tumour angiogenesis, regulated by vascular endothelial growth factor and the angiopoietins. *J Theor Biol.*, 229(4):435–454, Aug 2004. URL `http://www.ncbi.nlm.nih.gov/pubmed/15246783`.

[26] K. Bentley, G. Marriggi, and H. Gerart. Tipping the balance: robustness of tip cell selection, migration and fusion in angiogenesis. *PLoS Comput Biol*, 5(10):e1000549, October 2009. URL `http://www.ncbi.nlm.nih.gov/pubmed/19876379`.

[27] T. A. M. Heck, M. M. Vaeyens, and H. Van Oosterwyck. Computational models of sprouting angiogenesis: merits and future challenges. 2014.

[28] C. J. Slagera, J. J. Wentzel, F. J. H. Gijsen, J. C. H. Schuurbiers, A. C. van der Wal, A. F. W. van der Steen, and P. W. Serruys. The role of shear stress in the generation of rupture-prone vulnerable plaques. *Nature Clinical Practice Cardiovascular Medicine*, 2:401–407, August 2005.

[29] Jie Liu. Mechanotransduction in endothelial cells: Cell growth, angiogenesis and wound healing. 2010. URL `https://etd.ohiolink.edu/rws_etd/document/get/osu1274392778/inline`.

[30] Y. T. Shiu, J. R. A. Weiss, J. B. Hoying, M. N. Iwamoto, I. S. Joung, and C. T. Quam. The role of mechanical stresses in angiogenesis. *Critical Reviews^{TM} in Biomedical Engineering*, 33(5):431–510, 2005.

[31] J. P. Califano and C. A. Reinhart-King. A balance of substrate mechanics and matrix chemistry regulates endothelial cell network assembly. *Cellular and Molecular Bioengineering*, 1:122–132, October 2008.

[32] R. F. M. van Oers, E. G. Rens, D. J. LaValley, and C. A. Reinhart-King. Mechanical cell-matrix feedback explains pairwise and collective endothelial cell behavior in vitro. *PLOS Comput Biol*, 10(8):e1003774, August 2014. URL `http://www.ploscompbiol.org/article/fetchObject.action?uri=info%3Adoi%2F10.1371%2Fjournal.pcbi.1003774&representation=PDF`.

[33] Chris Green. Computer simulation integral in the diagnosis, treatment or prevention of disease by the end of the century., 2014. URL `http://goo.gl/9FbK0S`. [Online; accessed 20-September-2014].

[34] A. Prosperetti and G. Tryggvason. *Computational Methods for Multiphase Flow*. Cambridge, New York, p. 1-14, 2009.

[35] C. A. Reinhart-King, M. Dembo, and D. A. Hammer. Endothelial cell traction forces on rgd-derivatized polyacrylamide substrata. *Langmuir*, 19:1573–1579, 2003. URL `http://www.cellmechanics.org/downloads/Reinhartking_Langmuir_2003.pdf`.

[36] A. L. Correia. *Influence of Tissue Mechanics in Blood Vessel Growth*. MSc thesis, Universidade de Coimbra, 2012.

[37] W. Feneberg, M. Aepfelbacher, and E. Sackmann. Microviscoelasticity of the apical cell surface of human umbilical vein endothelial cells (huvec) within confluent monolayers. *Biophys J.*, 87(2):1338–1350, August 2004. URL `http://www.ncbi.nlm.nih.gov/pubmed/15298936`.

[38] J. P. Califano and C. A. Reinhart-King. The effects of substrate elasticity on endothelial cell network formation and traction force generation. *Conf Proc IEEE Eng Med Biol Soc.*, 2009:3343–3345, September 2009. URL `http://www.ncbi.nlm.nih.gov/pubmed/19964074`.

[39] C. B. Raub, A. J. Putnam, B. J. Tromberg, and S. C. George. Predicting bulk mechanical properties of cellularized collagen gels using multiphoton microscopy. *Acta Biomater.*, 6(12):4657–4665, December 2010. URL `http://www.ncbi.nlm.nih.gov/pubmed/20620246`.